

Orientation Tuning of Input Conductance, Excitation, and Inhibition in Cat Primary Visual Cortex

JEFFREY S. ANDERSON,¹ MATTEO CARANDINI,¹⁻³ AND DAVID FERSTER¹

¹*Department of Neurobiology and Physiology, Northwestern University, Evanston, Illinois 60208;* ²*Howard Hughes Medical Institute and Center for Neural Science, New York University, New York, New York 10003; and* ³*Institute of Neuroinformatics, Swiss Federal Institute of Technology and University of Zurich, CH-8057 Zurich, Switzerland*

Received 10 January 2000; accepted in final form 5 May 2000

Anderson, Jeffrey S., Matteo Carandini, and David Ferster. Orientation tuning of input conductance, excitation, and inhibition in cat primary visual cortex. *J Neurophysiol* 84: 909–926, 2000. The input conductance of cells in the cat primary visual cortex (V1) has been shown recently to grow substantially during visual stimulation. Because increasing conductance can have a divisive effect on the synaptic input, theoretical proposals have ascribed to it specific functions. According to the veto model, conductance increases would serve to sharpen orientation tuning by increasing most at off-optimal orientations. According to the normalization model, conductance increases would control the cell's gain, by being independent of stimulus orientation and by growing with stimulus contrast. We set out to test these proposals and to determine the visual properties and possible synaptic origin of the conductance increases. We recorded the membrane potential of cat V1 cells while injecting steady currents and presenting drifting grating patterns of varying contrast and orientation. Input conductance grew with stimulus contrast by 20–300%, generally more in simple cells (40–300%) than in complex cells (20–120%), and in simple cells was strongly modulated in time. Conductance was invariably maximal for stimuli of the preferred orientation. Thus conductance changes contribute to a gain control mechanism, but the strength of this gain control does not depend uniquely on contrast. By assuming that the conductance changes are entirely synaptic, we further derived the excitatory and inhibitory synaptic conductances underlying the visual responses. In simple cells, these conductances were often arranged in push-pull: excitation increased when inhibition decreased and vice versa. Excitation and inhibition had similar preferred orientations and did not appear to differ in tuning width, suggesting that the intracortical synaptic inputs to simple cells of cat V1 originate from cells with similar orientation tuning. This finding is at odds with models where orientation tuning in simple cells is achieved by inhibition at off-optimal orientations or sharpened by inhibition that is more broadly tuned than excitation.

INTRODUCTION

One of the properties that most profoundly affects the computation performed by a neuron is its input conductance. If the input conductance remains substantially constant, the neuron integrates its synaptic inputs linearly with excitation providing an additive term and inhibition providing a subtractive term. By contrast, increases in input conductance have a divisive effect on synaptic inputs and thus introduce a nonlinearity into the neuron's computation.

In the primary visual cortex (V1), the input conductance has been invoked explicitly by two different models of cortical function. In their veto model, Koch and Poggio (1985) proposed that a cell's conductance should be highest for the orientations that are most different from the cell's preferred orientation (Fig. 1A). Input conductance would then play an important role in sharpening the orientation tuning of V1 cells. The contrast normalization model (Carandini et al. 1997, 1999; Heeger 1992) posits that conductance should also grow with visual stimulation, but in a manner that is independent of stimulus orientation (Fig. 1B). In this view, the input conductance would provide a gain-control mechanism that decreases the responsiveness of the cells at high stimulus contrast.

Large increases in input conductance (up to 300%) were demonstrated in cortical neurons as long as 30 years ago (Dreifuss et al. 1969), both after electrical stimulation of the cortical surface and after iontophoretic application of GABA. Early measurements of input conductance during optimal visual stimulation, even with stimuli of optimal orientation, resulted in substantially lower estimates (Berman et al. 1991; Carandini and Ferster 1997; Douglas et al. 1988; Ferster and Jagadeesh 1992; Pei et al. 1991). More recently, however, large visually evoked conductance increases have been reported (Borg-Graham et al. 1998; Hirsch et al. 1998). We have therefore recorded intracellularly from simple and complex cells in cat V1 while stimulating with drifting gratings and made precise measurements of the orientation tuning and contrast response of visually evoked changes in conductance.

We found, as did Borg-Graham et al. (1998) and Hirsch et al. (1998), that input conductance grows by 20–300% with stimulus contrast and can show substantial temporal modulation during the responses to optimal drifting gratings. Moreover we found the input conductance of all cells to vary with the orientation of the drifting gratings, with the maximal conductance occurring in response to stimuli of the preferred orientation (Fig. 1C). Our results therefore run opposite to what would be predicted by the veto theory. Our results are also at odds with a key aspect of the contrast normalization model: while conductance increases could provide the cells with a divisive gain control mechanism, this mechanism would be orientation selective and thus not depend purely on visual

Address for reprint requests: D. Ferster, Dept. of Neurobiology and Physiology, Northwestern University, 2153 N Campus Dr., Evanston, IL 60208 (E-mail: ferster@northwestern.edu).

The costs of publication of this article were defrayed in part by the payment of page charges. The article must therefore be hereby marked "advertisement" in accordance with 18 U.S.C. Section 1734 solely to indicate this fact.

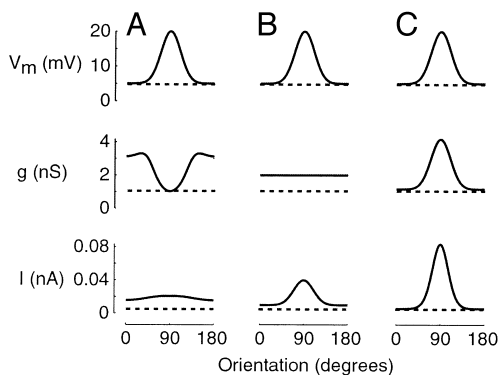


FIG. 1. Cartoon of 3 possible effects of input conductance on the orientation tuning of cat V1 cells. The 3 effects correspond to those postulated by the veto model, by the normalization model, and that measured in the present study.

contrast. Our results agree with conductance changes predicted by a feedforward model of cat simple cell function that includes a spatial push-pull arrangement of on and off excitation and inhibition (Troyer et al. 1998).

In addition to measuring the total input conductance, we have also attempted to distinguish the components of the conductance changes arising from excitatory and inhibitory synaptic inputs. This distinction is based on the assumption that the changes in input conductance are entirely synaptic. Using this approach, we studied the orientation tuning of synaptic excitation and inhibition and found that they were similar. This similarity would be predicted if intracortical excitation and inhibition originated from cells with similar orientation tuning and would explain previous reports that orientation tuning is not sharpened by intracortical inhibition (Chung and Ferster 1998; Ferster 1986; Ferster et al. 1996; Nelson et al. 1994).

Some of these results have been presented elsewhere in abstract form (Carandini et al. 1998a–c).

METHODS

Experimental preparation

Details of the experimental preparation have been described previously (Ferster and Jagadeesh 1992; Jagadeesh et al. 1997). Young adult cats were anesthetized with intravenous thiopental sodium and placed in a stereotaxic headholder. Either gallamine or pancuronium was given to minimize motion of the eyes, and the animals were artificially respired. Phenylephrine hydrochloride and atropine sulfate were applied to the eyes to retract the nictitating membranes, dilate the pupils, and paralyze accommodation. Contact lenses with artificial pupils (4 mm diam) were inserted.

Visual stimulation

Visual stimuli consisted of drifting sine-wave gratings displayed on a Tektronix 608 oscilloscope screen using a Picasso stimulus generator (Innisfree, Cambridge, MA). The peak contrast used was 64% and the mean luminance was 20 cd/m². Stimuli lasted 4 s. The spatial frequency, drift rate, and spatial position of the gratings were optimized under computer control. An orientation of 0° corresponds to a vertical grating moving to the right; an orientation of 90° corresponds to a horizontal grating moving downward.

Input conductance was measured by recording the membrane potential responses to visual stimuli while injecting, in turn, 3–11

different steady currents, I_{inj} . Stimuli were grouped in blocks of 12 different orientations at 64% contrast (or 7 different contrasts at preferred orientation for experiments measuring contrast responses) together with one blank stimulus, all presented in random order. Blocks were repeated with different random orders and with different injected currents, which were held constant for an entire stimulus block. The currents, ranging from –350 to 200 pA, were most often negative, to minimize spiking and other effects of voltage-dependent membrane nonlinearities.

Intracellular recording

Whole cell patch recordings were obtained from neurons of area 17 of the visual cortex using the technique developed for brain slices by Blanton et al. (1989). Electrodes were filled with a K⁺-gluconate solution including Ca²⁺ buffers, pH buffers, and cyclic nucleotides as described by Spruston et al. (1995). Membrane potentials, recorded with an Axoclamp amplifier (Axon Instruments, Burlingame, CA) in current-clamp (bridge) mode, were low-pass filtered and digitized at 4 kHz (visually evoked records) or 15 kHz (electrically evoked records). To compensate for junction potentials (Neher 1992), an electrode was placed in a bath of artificial cerebrospinal fluid (ACSF), which was gradually replaced with a solution that more resembled intracellular ionic concentrations. The resulting 10-mV change in measured potential was subtracted from all recordings. Electrical stimuli to the lateral geniculate nucleus (LGN) consisted of 1.0-mA pulses, 200 ms in duration, electrode negative.

Cells were classified as simple or complex on the basis of the presence or absence of ON and OFF subregions in the receptive field and by the ratio of mean to modulation of the membrane potential response to drifting gratings optimized for orientation, spatial frequency, and drift frequency (Carandini and Ferster 2000; Skottun et al. 1991). Modulation is computed as twice the amplitude of the response component at the frequency of the drifting grating (1, 2, or 4 Hz).

Compensation for electrode resistance

The capacitance and resistance (4–15 M Ω) of the electrodes were easily neutralized before patching a cell. When a patch was obtained, however, the electrode resistance R_e increased dramatically. The resistance of the electrode after the patch is formed is also known as the access or series resistance, and its value must be properly neutralized to measure input conductance accurately. To this end, we employed a series of three methods, one qualitative, performed during the recording, and the other two quantitative, performed off-line.

To measure electrode resistance by eye, –100-pA current pulses were injected into the cell. In the standard method, the faster decay component in the response, reflecting the electrode's time constant, is then distinguished from the slower component, reflecting the cell's time constant. The amplifier bridge is then balanced to neutralize the electrode component for the purposes of recording. This method gives only an approximate value for series resistance, however, given the similarity of the time constants of the two components of *in vivo* patch recordings.

The first quantitative method for estimating the electrode resistance was based on off-line fitting of the responses to current pulses of several different amplitudes. We injected a series of current steps periodically throughout the course of a recording, and we fitted them with the predictions of a simple model. In the model, we considered the patched electrode and the cell membrane to be simple resistor-capacitor circuits arranged in series. The response $V(t)$ of such a model to a step of injected current I_{inj} is given by a double exponential

$$V(t)/I_{inj} = R_e[1 - \exp(-t/\tau_e)] + R_m[1 - \exp(-t/\tau_m)] \quad (1)$$

where R_e and τ_e are the resistance and time constant of the patched electrode, and R_m and τ_m are the resistance and time constant of the

cell membrane. The model was fitted to the responses to a series of current pulses, usually 40 pulses of eight different amplitudes ranging from -0.3 to 0.2 nA presented at $1-2$ Hz, with each pulse lasting about 100 ms. The total resistance $R_e + R_m$ was calculated from the average potential reached at steady state (after 100 ms), and the remaining three parameters, R_e , τ_e , and τ_m , were estimated by least square fitting of Eq. 1 to the data.

This estimation is illustrated in Fig. 2, A–D. The responses to each current pulse (A) were divided by the injected current, and the resulting responses (B) were fitted with Eq. 1. In every case a clear minimum in the error function was found. An example is illustrated in C, which shows the error corresponding to each pair of values R_e and τ_e , and to the corresponding best estimate of τ_m . The estimated contribution $I_{inj} R_e$ of the electrode to the recorded potential was then subtracted from the traces to yield the estimated true membrane potential response (D). Because the main measurements in this study were obtained with steady current injections, we did not need to further compensate for the electrode time constant.

The reliability of these estimates was assessed in two ways. First, we applied the fitting procedure to simulated data obtained from Eq. 1 with added noise. We found the estimated parameters to be accurate to within 0.5% of the correct values. Second, we performed each fitting procedure on 500 randomly selected subsets of the current pulses from a single complete set (Efron and Tibshirani 1993). The resulting 95% confidence intervals for the estimated parameters were between 2 and 10% for resistance values and less than 1% for time constants.

The second quantitative method for estimating the electrode resistance was based on the assumption that the threshold for action potential generation V_{thr} should be largely independent of the injected current I_{inj} . This assumption is justified because our injected current was constant (Koch 1999). Any effect of injected current on the measured threshold should then be ascribed to the electrode resistance.

The application of this technique is illustrated in Fig. 2, E–H. After R_e had been neutralized according to the double exponential fitting technique, we compared spike thresholds, taken to be the minimum

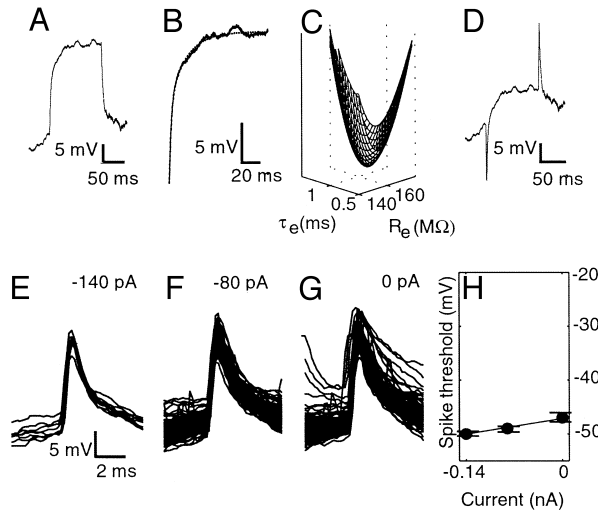


FIG. 2. Techniques used to estimate and compensate for the electrode resistance. A: Recorded response to a current pulse (0.1 nA, average of 3 traces). B: detail of the response with fit provided by model in Eq. 1 (---). C: mean square error in fit for different values of electrode resistance and time constant. D: response to the current pulse after subtraction of the estimated electrode contribution $I_{inj} R_e$. E–G: spikes recorded while injecting different steady currents I_{inj} . Potentials have been corrected for R_e obtained from the double-exponential fitting technique. H: minimum spike thresholds as a function of the injected current I_{inj} . Error bars indicate 1 SE across stimulus presentations. Line represents best linear fit through the points. The slope of this line most likely reflects a residual component R_a of the electrode resistance that was not properly neutralized by exponential fitting method. Cell 16.

potential at which a spike was generated, at different I_{inj} (E–G). On the assumption that the actual V_{thr} was unchanged by current injection, any apparent change in V_{thr} would represent a resistive component in the patch electrode that had not been properly neutralized. Even though these potentials had been corrected for R_e as calculated from the double exponential fitting procedure, the measured threshold varied with the injected current. A linear fit to the relationship between V_{thr} and I_{inj} yields R_a , the difference between the values of R_e obtained from the exponential fitting and threshold estimation techniques (H).

The two independent methods used to estimate R_e were in close agreement (within 15%) for all cells, close to the level of precision estimated for the two techniques. The values for the electrode and membrane resistance R_e and R_m estimated from the exponential fitting technique, as well as the residual electrode resistance R_a obtained from the threshold estimation technique are reported in Table 1 for all cells tested with visual stimuli. Final values of R_e were taken to be the mean of the values obtained from the two techniques. Changes in R_e were tracked over the course of a recording. Values were linearly interpolated over time between measurements and applied to individual records of visually evoked responses. Drifts in R_e were always less than 10% in amplitude.

Tuning curves

On various occasions we consider the orientation tuning curves of various measures of cell responses, such as membrane potential or input conductance. The amplitudes of these responses as a function of orientation were fit with a simple function consisting of a sum of two Gaussians. The two Gaussians are forced to peak 180° apart, and to have the same width σ :

$$f(O) = \Psi_0 + \Psi_p e^{-(O-O_p)^2/(2\sigma^2)} + \Psi_n e^{-(O-O_p+180)^2/(2\sigma^2)} \quad (2)$$

In the above expression, O is the stimulus orientation, and angular brackets indicate orientation values between -180 and 180° . The function has five parameters: the preferred orientation O_p , the response at the preferred orientation Ψ_p , the response at 180° from the preferred orientation as the preferred but with nonpreferred direction), the response in the absence of visual stimuli Ψ_0 , and the tuning width σ (Carandini and Ferster 2000).

Bootstrap estimates for conductance

To assess the reliability of conductance measurements, we used the bootstrap method (Efron and Tibshirani 1993). We randomly selected $1,000$ subsets (with repetition allowed) of the traces used to calculate input conductance. Each subset contained the same number of elements as the total number of traces used to calculate input conductance. Subsets were required to contain traces representing at least three different levels of injected current. For each subset, the data at each point in time were fit to a line (Eq. 3) to obtain values of $g(t)$. To construct 95% confidence intervals, the 2.5 and 97.5 percentiles were selected from the $1,000$ values for $g(t)$ at each point in time.

RESULTS

We report here on data from 24 cells selected from a total of 49 that were recorded with multiple injected currents. These cells met or exceeded the following minimal requirements: that their visual response properties were well characterized (orientation, spatial frequency, and temporal frequency preferences); that they had action potentials greater than 10 mV in amplitude; (spikes are often of smaller amplitude for in vivo whole cell recordings than in sharp microelectrode recordings due to filtering by higher electrode resistances); that their

TABLE 1. Summary of the properties of the cells in this study

Cell	Type	Parameter ^a	V_{rest} , mV ^b	V_{thr} , mV ^c	τ_m , ms ^d	R_m , M Ω ^e	R_a , M Ω ^f	R_e , M Ω ^g	No. of Currents ^h	Max Δg , % ⁱ
1	Simple	Orientation	-73	-68	19.7	57	10	83	3	140
		Contrast	-70	-65	19.7	57	2.3	83	3	282
2	Simple	Orientation	-68	-54	15.2	85	-3	94	3	89
		Contrast	-72	-58	15.2	85	-3	94	3	106
3	Simple	Orientation	-63	-54	20.0	52	-22	168	5	42
4	Simple	Orientation	-58	-55	15.7	30	-15	107	8	330
5	Simple	Orientation	-50	-41	15.4	143	14	200	8	70
		Contrast	-50	-44	15.4	143	15.5	200	8	43
6	Simple	Orientation	-72	-61	N/A ^f	130	N/A ^j	N/A ^j	3	75
7	Simple	Orientation	-61	-40	16.5	101	20	132	5	68
8	Simple	Contrast	-67	-39	17.3	56	0.5	89	3	315
9	Simple	Contrast	-62	-55	22.0	43	10	172	3	213
10	Complex	Orientation	-70	-61	18.1	30	0.2	107	11	62
11	Complex	Orientation	-73	-54	10.6	72	2	193	5	60
12	Complex	Orientation	-63	-53	7.0	58	5	150	5	122
13	Complex	Orientation	-80	-65	13.6	52	10	132	5	22
14	Complex	Contrast	-68	-50	11.9	72	23.1	160	7	64

^a Parameter indicates the stimulus parameter that was varied to measure the effects of visual stimulation on input conductance. ^b V_{rest} is the mean membrane potential when stimulus is a blank screen (for orientation experiments) or a 1% contrast grating (for contrast experiments). ^c V_{thr} is the threshold of the action potentials. ^d τ_m is the membrane time constant. ^e R_m is the input resistance. ^f R_a is the residual access resistance (after balancing the bridge online and performing double-exponential fit) estimated from the spike thresholds. ^g R_e represents the electrode resistance. ^h No. of currents lists how many different injected current levels were used for each analysis. ⁱ The last column indicates the maximum percentage conductance increase over baseline obtained in response to visual stimuli. ^j For cell 6, the bridge was balanced using the spike threshold technique only.

access resistance was less than 200 M Ω ; and that we were able to record the responses to a complete set of visual or electrical stimuli for at least three different injected currents (including the 0-current condition). Fourteen of the 23 cells (9 simple, 5 complex) were tested with current injection paired with visual stimulation. A summary of the properties of these cells is given in Table 1. Eleven of the 24 cells (3 simple, 8 complex) were tested with current injection paired with electrical stimulation in the LGN. One cell was tested with both visual and electrical stimulation.

Visually evoked responses of one simple cell are illustrated in Fig. 3. The visual stimulus was a drifting sinusoidal grating optimized for orientation, spatial frequency and drift rate. These responses are in line with previous observations (Jagadeesh et al. 1993): the 1% contrast grating (*top*) did not evoke any noticeable response, whereas the 64% contrast grating (*bottom*) evoked approximately sinusoidal membrane potential modulations, with action potentials rising from the peaks. These modulations had the same frequency as the drift rate of the stimulus, and resulted in a spike train that was strongly modulated at the same frequency. Injecting negative (-300 pA, *left*) or positive (140 pA, *right*) steady currents during the stimulus presentation had the predictable effect of hyperpolarizing or depolarizing the membrane. The current-induced changes in membrane potential were greater during the low-contrast stimulus (*top*) than during the high-contrast stimulus (*bottom*). This difference indicates a decrease in conductance at high contrasts. Differences like these form the basis for quantitative measurements of visually evoked conductance changes.

Measurement of input conductance

The effect of current injection on the membrane potential is more evident in Fig. 4B, where responses were averaged cycle by cycle and low-pass filtered. The thick traces show the

membrane potential responses in the absence of current injection and the thin traces above and below them indicate the responses in the presence of positive and negative injected current. As in the individual traces, the vertical distance between the averaged traces is larger for the low-contrast stimulus than it is for the high-contrast stimulus. To quantify this

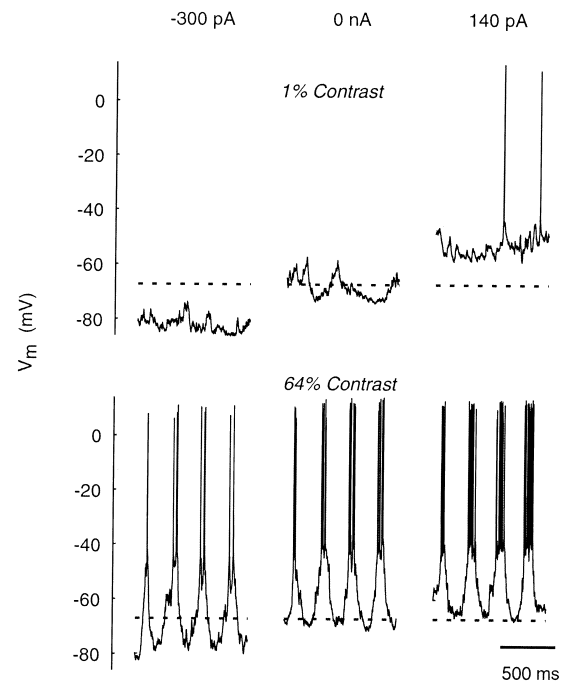


FIG. 3. Responses of a simple cell during visual stimulation and steady current injection. The visual stimulus was a drifting sinusoidal grating optimized for orientation, spatial frequency, and drift rate. The different panels show responses to 2 stimulus contrasts (1%, *top* and 64%, *bottom*), and 3 steady current injections (*left to right*: -300, 0 and 140 pA). \cdots , the resting membrane potential V_{rest} in the absence of current injection. The first 2 s of the responses are shown here (stimuli lasted 4 s). Cell 8.

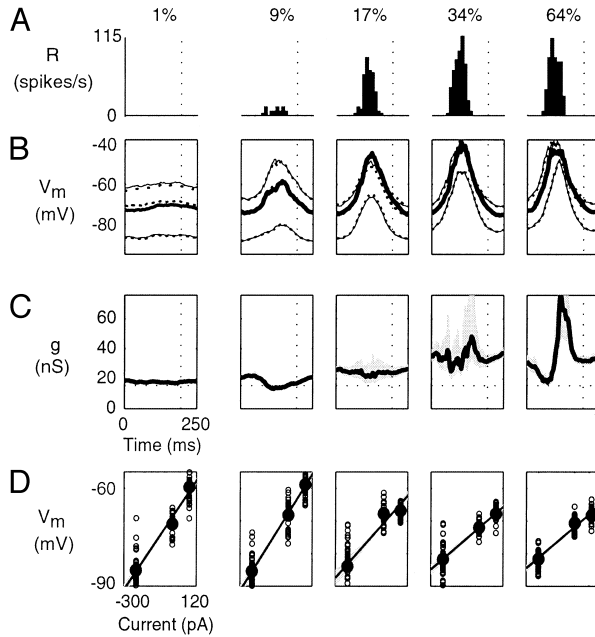


FIG. 4. Measurement of the input conductance at 5 different stimulus contrasts. Columns correspond to a different contrasts, from 1% (left) to 64% (right). *A*: average of the spike responses during a stimulus cycle in the absence of current injection. *B*: membrane potential responses. Thick trace is membrane potential in the absence of current injection ($I_{inj} = 0$). Continuous traces above and below are the potentials with $I_{inj} = 140$ pA and $I_{inj} = -300$ pA. Dotted traces indicate the linear prediction for these potentials. Horizontal reference line is V_{rest} . *C*: input conductance $g(t)$. Gray area represents 95% confidence interval. Dotted line indicates the mean conductance at rest, g_{rest} . *D*: estimation of input conductance at 1 point in time during the cycle ($t = 200$ ms, vertical lines in *A–C*). Abscissa is injected current I_{inj} . Symbols are the membrane potential responses in the individual cycles (open circle) and their means over all cycles (filled circle). Fitted lines are from Eq. 3, with the conductance g as the sole free parameter. Gray area represents 95% confidence interval on the slope. Cell 8.

effect, at each time in the cycle the relation between the injected current and the membrane potential was fitted with a line

$$V(t) = V_{visual}(t) + I_{inj}/g(t) \quad (3)$$

where $g(t)$, the inverse of the slope of the line, is the input conductance at time t . The intercept of the line is the mean membrane potential in the absence of current injection ($I_{inj} = 0$). We refer to the intercept as $V_{visual}(t)$, a linear estimate of the membrane potential recorded without injected current. This procedure is illustrated for time $t = 200$ ms, in Fig. 4*D* where the open symbols are the membrane potential, $V(t)$, recorded in individual trials, and the closed symbols are their means.

To assess the time course of changes in input conductance, we calculated a fit to Eq. 3 at each time, t , in the stimulus cycle. An estimate of the quality of these fits can be obtained by constructing a series of linear predictions for the potential in the presence of injected currents. That is, for each injected current and at each moment in time, we predicted the membrane potential from the corresponding fit to Eq. 3. The quality of these predictions can be judged in Fig. 4*B* by comparing the dotted curves with the continuous curves. The fits exhibit some systematic errors but are in general satisfactory, indicating that in this range of potentials and signal frequencies the membrane is acting approximately linearly.

It thus becomes possible to model the behavior of the cell

with a single value of conductance at each point in time, as illustrated in Fig. 4, *C* and *D*. Using this method, we see that for the simple cell in Fig. 4, the input conductance rose from around 20 nS for very low contrast stimuli (1%) to more than 80 nS for high contrast stimuli (64%). This corresponds to a 330% conductance increase. For some stimulus contrasts, moreover, the increase in conductance could be strongly modulated at the drift frequency of the stimulus. For example, the conductance increases elicited by the 64% contrast grating were largely confined to an interval immediately following the peak of the membrane potential responses. The 17% contrast grating, instead, elicited increases in conductance that were smaller but largely constant over the stimulus presentation time. At no time and for no stimulus contrast was the conductance ever smaller than at the resting condition.

We will see that all the other simple cells in our sample displayed similarly large, modulated conductance increases, in the range of 40–300%, whereas complex cells showed smaller (20–100%) conductance increases that were generally constant in time.

Reliability of the measurements

The value of these observations on the input conductance depends, of course, on the reliability of our measurements. To measure this reliability we computed 95% confidence intervals for the conductance, obtained from bootstrap estimates of the slope of the lines relating I_{inj} and V , such as those in *D*. These confidence intervals are indicated by the gray areas around the conductance traces in *C* and around the fitted lines in *D*. The gray areas are quite small even in the face of substantial spread in the membrane potential distributions, and indicate that we can trust our estimation of the input conductance.

Another important issue is whether the linear model described in Eq. 3 provided satisfactory fits in the tested range of membrane potentials. As described in the preceding text, the quality of the fits can be observed directly in Fig. 4*B*, where the membrane potentials predicted by the model are compared with the actual recorded membrane potentials. It can also be estimated statistically by comparing the actual membrane potential to the predicted membrane potential for the entire data set obtained from this cell. The density plot in Fig. 5 summarizes 9,408 data points, as in this data set there were 12 samples during each cycle (after low-pass filtering), 16 cycles per stimulus, seven stimulus contrasts, and seven presentations of the stimulus set (3 with $I_{inj} = -300$ pA, 2 with $I_{inj} = 0$ pA and 2 with $I_{inj} = 140$ pA). The horizontal streaks result from the trial-to-trial variability in the actual responses for a given stimulus condition. Overall, the linear model (Eq. 3) accounted for 85% of the variance in this data set. A comparable degree of accuracy was common in our sample ($77 \pm 44\%$ of the variance; mean \pm SE).

An accurate prediction of membrane potential responses by Eq. 3 requires that the omitted capacitive term, $C \cdot dV/dt$, be small. This term is required for a mathematically exact description of the changes in membrane potential. In the case of visually evoked responses, however, dV/dt is negligible (1,000 times smaller than it is during action potentials, for example). We found that including the $C \cdot dV/dt$ term changed the predicted membrane potentials by less than 2%.

Considering the nonlinearities that exist in cortical cells,

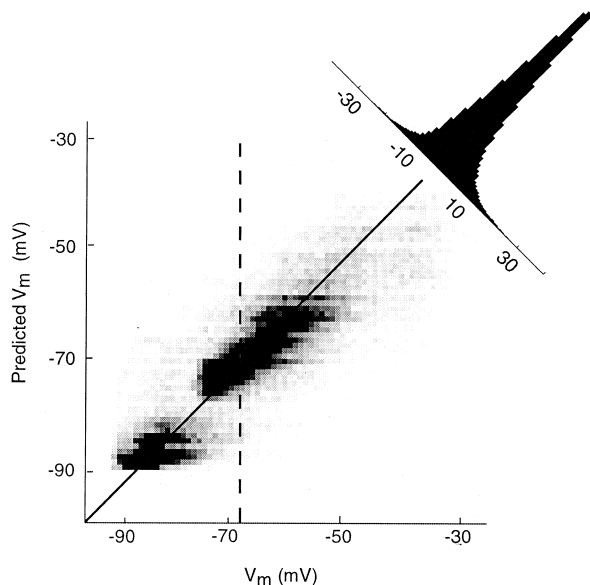


FIG. 5. Quality of the linear fits to the data. The abscissa indicates the actual recorded value of the membrane potential, and the ordinate indicates the value predicted by fits of the linear model (Eq. 3). Graph shows density plot with 1-mV binwidth. Vertical reference line indicates V_{rest} . The model accounted for 85% of the variance. If it accounted for 100% of the variance, all the dots would lie on the diagonal line. Inset (top right) shows a histogram of $V_m - \text{Predicted } V_m$ for all data points. Cell 8.

such as voltage-dependent channels (Koch 1999), this performance may be considered surprising. Part of the explanation may lie in our having chosen mostly small, negative injected currents, a choice that was made expressly to minimize the activation of voltage dependent conductances at depolarized potentials. Indeed, while Fig. 5 shows that the model did not perform worse at high values of the membrane potential than at low values, it may be that forcing the potential much above threshold by using larger positive injected currents would have revealed substantial nonlinearities.

Contrast dependence of conductance changes

Having established a method for estimating the conductance at each point in time during a stimulus, we can now measure the dependence of visually evoked changes in conductance on stimulus parameters such as orientation and contrast. The dependence of input conductance on contrast for the cell in Fig. 4, as well as for four other simple cells, is illustrated in Fig. 6. To quantify the changes in input conductance observed during visual stimulation, we have focused on two measures. The first is the *mean* conductance, and the second is the *modulation* of the conductance, which is taken to be twice the amplitude of the Fourier component of the response at the frequency of the drifting grating. Thus for a sinusoidal response, modulation represents the peak-to-peak amplitude of the response. These two measures are commonly used to characterize the firing rate responses (e.g., Movshon et al. 1978) and the membrane potential responses (Carandini and Ferster 1997, 2000) of simple cells to drifting gratings. Both mean and modulation of the input conductance are shown in Fig. 6C, and both of them increase in all cells as a function of stimulus contrast.

These increases in mean and modulation of the input conductance are similar but not identical to concurrent increases in

the firing rate and membrane potential responses (Fig. 6, A and B). For example, in the cell from Fig. 4 (Fig. 6, 4th column), contrasts as high as 17% elicited substantial firing rate and membrane potential responses, but did not elicit a significant conductance increase. The two highest contrasts, 34 and 64%, elicited very similar membrane potential (and firing rate) responses but different conductance increases.

Complex cells also showed increases in conductance with visual stimulation; these increases, however, were a third to a half the size of conductance increases seen in simple cells (See Table 1 for comparison of maximal conductance increases). The increase in conductance for a complex cell is illustrated for different stimulus contrasts in Fig. 7. As with the simple cell in Fig. 4, conductance grew with visual stimulation, particularly once the contrast reached 17%. Like the membrane potential (Carandini and Ferster 2000), the average input conductance of the complex cell was essentially constant over the stimulus cycle. The maximal conductance increase was 64% from a baseline of 12.1 nS to a peak of 19.8 nS at 64% contrast.

Orientation tuning of the conductance changes

Up to now we have considered only the conductance changes evoked by gratings of the preferred orientation and direction of motion. We have seen that input conductance grows with stimulus contrast, but we have not determined whether it depends on other stimulus attributes. Now we report on our main result, that conductance changes are tuned for

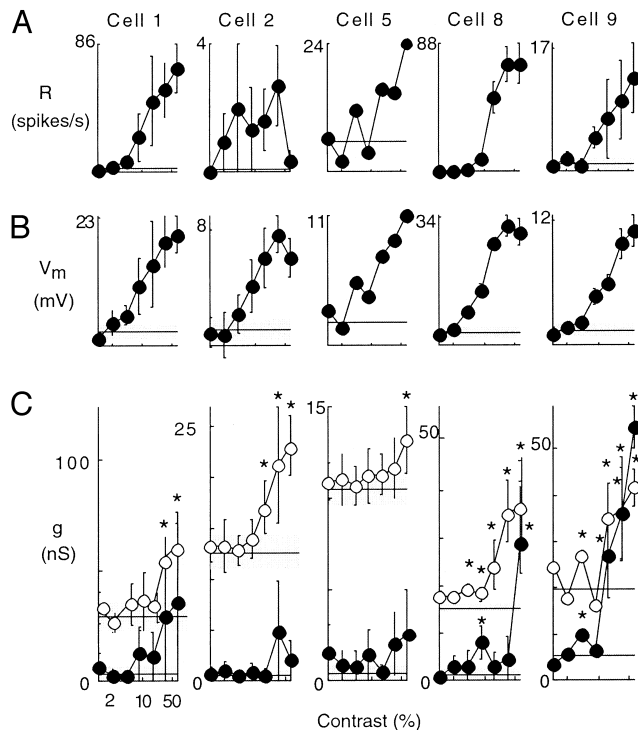


FIG. 6. Contrast dependence of firing rate, membrane potential, and input conductance for 5 simple cells. A: modulation of the firing rate responses. The modulations are peak-to-peak amplitudes of the best-fitting sinusoid having the same temporal frequency as the grating stimulus. B: modulation of the membrane potential responses. C: mean (\circ) and modulation (\bullet) of the input conductance. *, points significantly different from baseline; —, baseline values obtained with blank stimulus; \square , 95% confidence limits for baselines. Error bars represent the standard error of the mean.

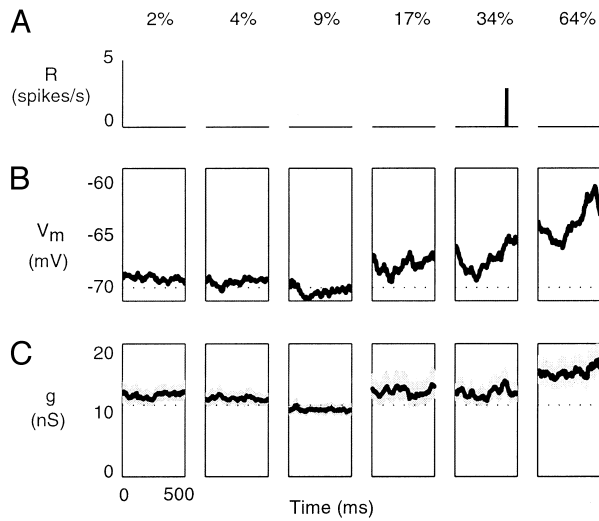


FIG. 7. Input conductance at different stimulus contrasts for a complex cell. Columns correspond to different contrasts, from 2% (*left*) to 64% (*right*). *A*: cycle averages of the spike responses (with $I_{inj} = 0$). *B*: cycle averages of the membrane potential responses, $V_{visual}(t)$. Horizontal reference line is V_{rest} . *C*: cycle averages of the input conductance $g(t)$. \square , 95% confidence intervals; \cdots , the mean conductance at rest, g_{rest} . Cell 14.

stimulus orientation: stimuli having a cell's preferred orientation, as defined by changes in membrane potential, elicit maximal conductance increases.

Examples of our results with stimuli of different orientations are illustrated for a simple cell in Fig. 8. The firing rate responses (*A*) and membrane potential responses (*B*) of the cell were tuned for orientations of approximately 120 and 300°, which correspond to identical orientations but opposite directions of motion. The firing rate responses of the cell exhibited

clear direction selectivity, being much stronger for stimuli drifting at 120° than for stimuli drifting at 300°. A glance at the cycle averages of the input conductance for each orientation (*C*) reveals the following two observations. First, at all orientations the conductance was higher than at rest (*far left* and \cdots in all panels). Second, the conductance increases were tuned for orientation and were strongest at the same orientations at which the firing rate and membrane potential responses were maximal.

Results from another simple cell are illustrated in Fig. 9. This cell was not particularly selective for stimulus direction and was tuned for orientations around 75°. The input conductance was similarly tuned and was substantially modulated over time. The timing of this modulation in input conductance was opposite to that of the firing rate and membrane potential responses: The maximal conductance consistently occurred during the trough of these responses. Other simple cells in our population showed similar behavior in that the maximum conductance was not simultaneous with the peaks in potential or in firing rate. Thus the conductance increases that we observe are unlikely to be related to the cell's approaching or reaching the threshold for action potential generation.

More generally, there was no simple relation between the input conductance of a simple cell and its membrane potential. For the cells in Figs. 4 and 9, the conductance consistently peaked at very different times than the membrane potential response. For the cell in Fig. 8, responses at preferred and nonpreferred orientations had similar mean values for membrane potential but nonoverlapping ranges for input conductance. In some simple cells, the membrane potential obtained with blank stimuli and with gratings drifting at nonpreferred orientations were quite similar, whereas conductance was sig-

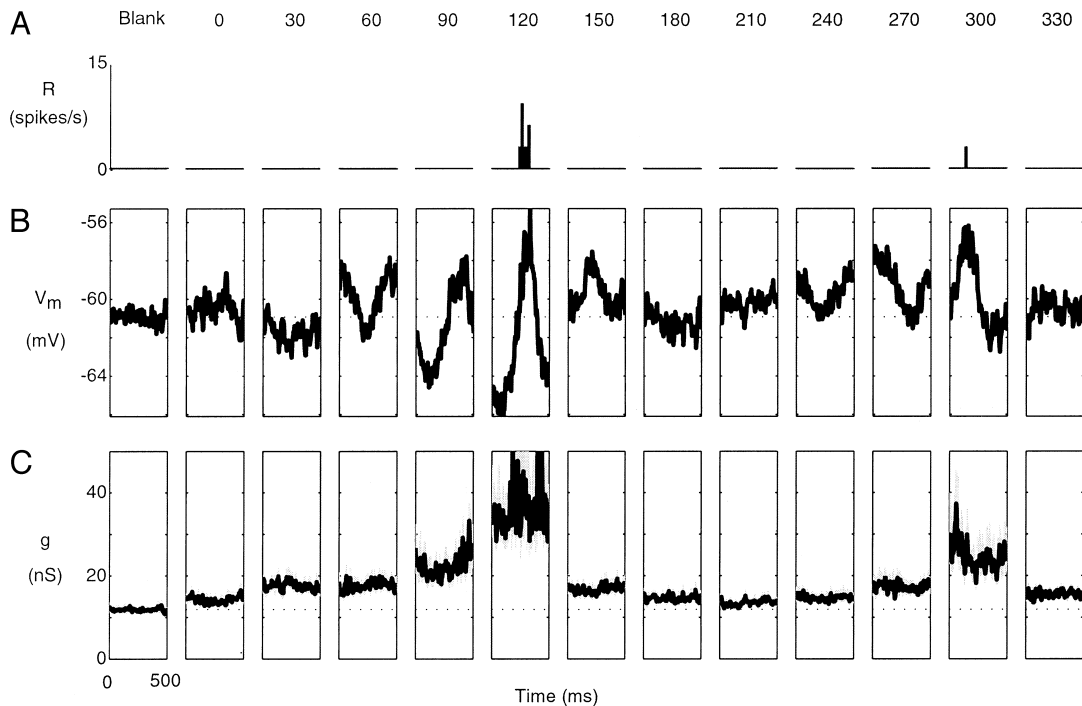


FIG. 8. Input conductance at different orientations for a simple cell. The 1st column corresponds to a blank stimulus (0% contrast), and each subsequent column to a different stimulus orientation. *A*: spike responses. *B*: membrane potential responses, $V_{visual}(t)$. \cdots , resting membrane potential V_{rest} . *C*: input conductance. \square , 95% confidence intervals; \cdots , the mean conductance at rest, g_{rest} . Cell 4.

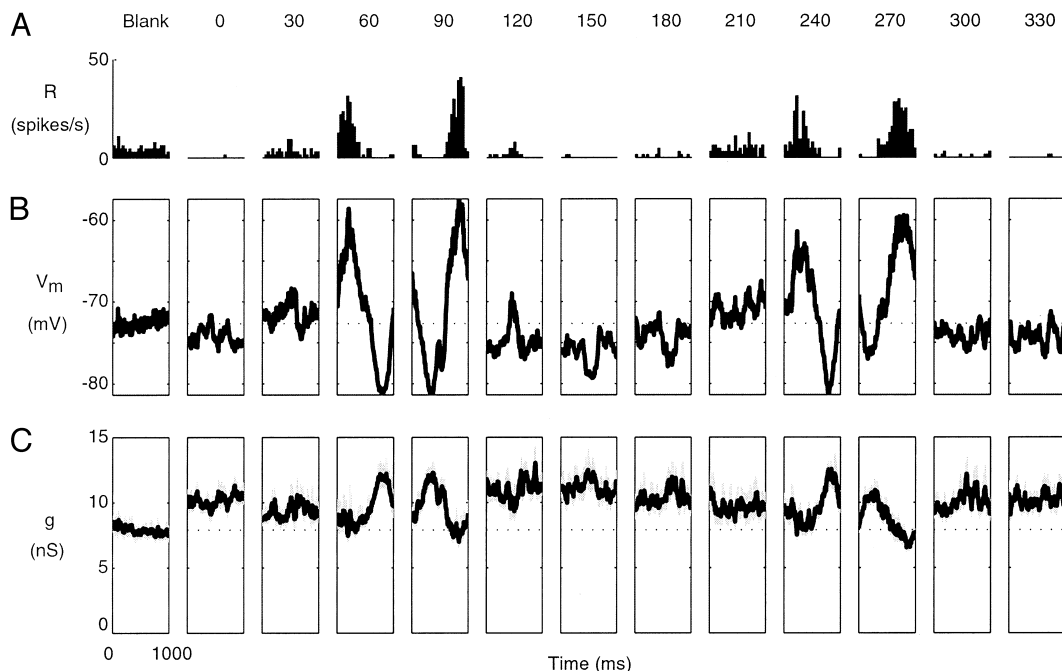


FIG. 9. Input conductance at different orientations for another simple cell. Format as in Fig. 8. *Cell 6*.

nificantly lower for recordings during blank stimuli. These considerations suggest that the observed changes in input conductance were not simply caused by intrinsic voltage-dependent channels in the membrane.

The orientation tuning of input conductance in simple cells was similar to that of the membrane potential. This similarity can be observed for seven simple cells in Fig. 10, where the tuning curves for conductance (*C* and *F*) are shown together with those for the firing rate (*A* and *D*) and membrane potential (*B* and *E*). Two components of the conductance changes are shown, the mean value (*C* and *F*: ○) and the size of the modulation in time (*C* and *F*: ●).

The tuning curves for the cell in Fig. 8 (*cell 4*) are among those illustrated in Fig. 10. In this cell the presence of a drifting grating elevated the mean input conductance (○) from a resting value of 10 nS to average values of about 16 nS for nonpreferred orientations and 29 nS for preferred orientations. Input conductance modulation (●) varied more than 10-fold with orientation, from around 0.4 to 10 nS peak to peak. The orientation tuning of the input conductance was very similar to that of the membrane potential. In contrast, the orientation tuning of the spike rate was significantly narrower (Carandini and Ferster 2000).

Analogous observations can be made for the cell in Fig. 9, whose orientation tuning is also illustrated in Fig. 10 (*cell 6*): in this cell the stimulus-driven increase in mean input conductance was not tuned, but the modulation in input conductance was clearly tuned. As with the previous cell, the modulation of input conductance peaked at the cell's preferred orientation.

Similar results apply to all remaining cells in Fig. 10: one or both components of the input conductance—mean and modulation—were well tuned for orientation. In *cells 1* and *6*, the mean component was not tuned for stimulus orientation, but the modulation component was strong and well tuned. In *cells 2* and *7*, the situation was reversed, where the modulation component was almost negligible, but the mean component

was strong and well tuned. In the remaining cells, both the mean and the modulation of the input conductance were well tuned for orientation.

The input conductance increases were also tuned for orientation in complex cells. As with simple cells, complex cells exhibited maximal conductance increases at the preferred orientation. In the cell in Fig. 11, for example, conductance increases of up to 60% were observed around the preferred orientation, which was between 270 and 300°. For the remaining orientations, conductance values were generally at or around baseline. Exceptions were common, however, such as occurs for this cell at 30°, which is roughly orthogonal to the preferred orientation. Whether or not these isolated increases in conductance at nonpreferred orientations are significant is somewhat difficult to determine because in complex cells the membrane potential traces and the associated conductance values were much more variable than in simple cells. The confidence limits in Fig. 11 are correspondingly larger in absolute terms than they are in Figs. 8 and 9, and the confidence limits for the trace at 30° nearly overlap with those at adjacent orientations. Figure 12 shows tuning curves of conductance, membrane potential and spike rate for this cell (*2nd column*) and for three additional complex cells.

To compare the orientation tuning of membrane potential and input conductance, we fitted the tuning curves in Fig. 10 with the descriptive function of Eq. 2 (METHODS). This function is the sum of two Gaussians that can have different heights but are constrained to peak 180° apart and to have identical widths. To minimize the number of tuning parameters, some constraints were imposed on the fits. First, the mean and modulation of the input conductance were fitted together, forcing them to peak at the same orientations and have the same tuning width. Second, the mean and modulation of the membrane potential were similarly fitted together. Third, the fits of the firing rate responses were obtained by requiring that they peak at the same orientation as the membrane potential responses.

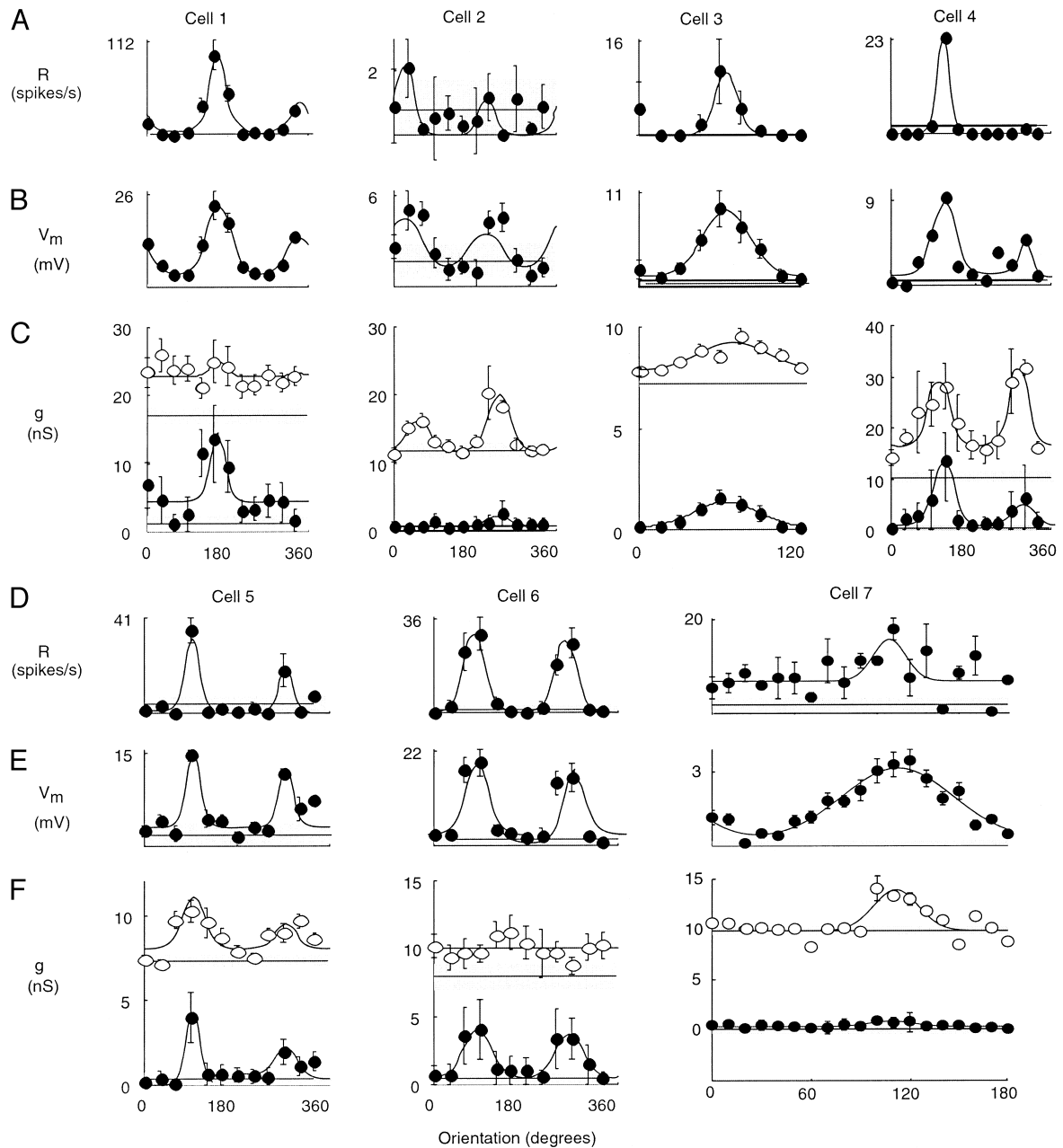


FIG. 10. Orientation tuning of the firing rate, of the membrane potential, and of the input conductance for 7 simple cells. Cells 3 and 7 were tested with a finer sampling for orientation than the other cells. Format for each set of panels (A–C and D–F) are as in Fig. 6. Curves fitted to data are a sum of 2 Gaussians (see METHODS.)

These requirements simplify the following analysis without significantly reducing the quality of the fits. Inspection of Fig. 10 reveals that the fits (—) closely approximate the data for simple cells. By contrast, the data from complex cells (not shown) were more noisy, and the fits were less satisfactory.

Preferred orientation and tuning widths derived from the tuning curves of Fig. 10 are compared in Fig. 13. The preferred orientation for the input conductance (A) was always close to the preferred orientation for the potential: the two differed in 7 of the 11 cells by less than 10° , and in all cells by less than 30° . Similarly, the tuning widths of the conductance increases were not significantly different from those of the membrane potential responses (B). For simple cells, the half-width at half-height of the functions fitted to the firing rate, membrane

potential, and input conductance were $16.9 \pm 2.6^\circ$, $28.8 \pm 4.2^\circ$, and $25^\circ \pm 2.2^\circ$ ($n = 7$). For complex cells, tuning width for firing rate, mean potential, and mean input conductance were $14.8^\circ \pm 4.1^\circ$, $18.6 \pm 3.8^\circ$, $17.8 \pm 4.4^\circ$ ($n = 4$). The narrower tuning width for firing rate can be easily explained by the presence of the spike threshold (Carandini and Ferster 2000; Chung and Ferster 1998).

Distinguishing excitation and inhibition

We have seen that visual stimulation can substantially increase the conductance of cortical neurons and that these conductance increases are not explained by membrane nonlinearities such as those involved in the generation of action

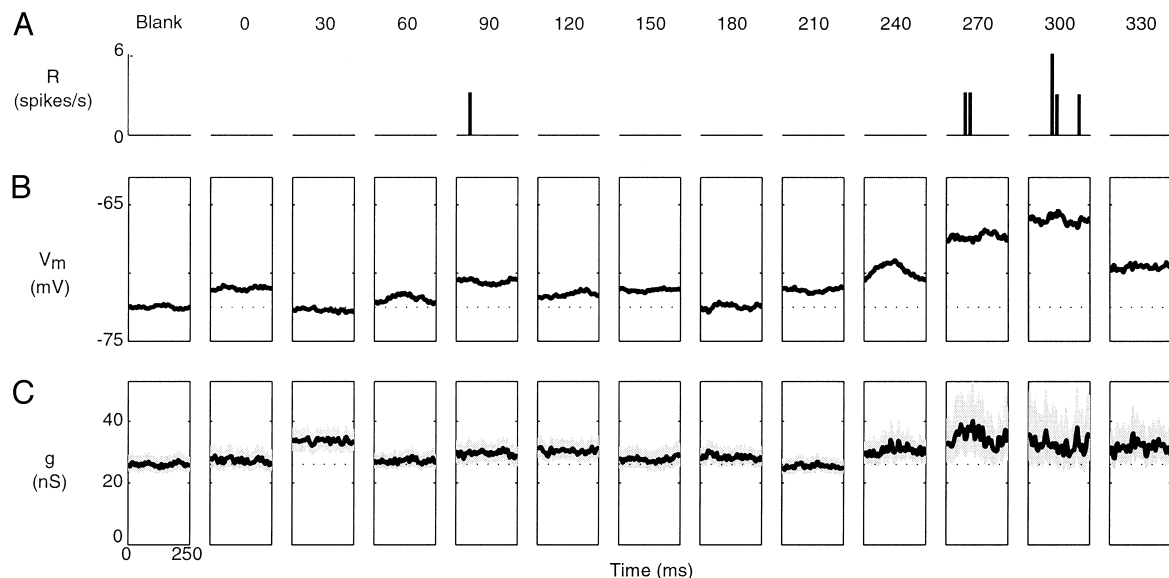


FIG. 11. Conductance changes as a function of stimulus orientation in a complex cell. Format as in Fig. 8. *Cell 11*.

potentials. What is the source of these conductance increases? The simplest explanation is that they are largely a consequence of increased synaptic activity. If this explanation were correct, it would be useful to determine how much of this synaptic conductance was excitatory and how much inhibitory.

On this assumption, we have attempted to derive from our data the time course and tuning of the excitatory and inhibitory synaptic inputs. We consider each neuron to have three conductances: an excitatory synaptic conductance $g_e(t)$, an inhibitory synaptic conductance $g_i(t)$, and a constant resting conductance g_{rest} . The sum of the three conductances is the total conductance

$$g(t) = g_e(t) + g_i(t) + g_{rest} \quad (4)$$

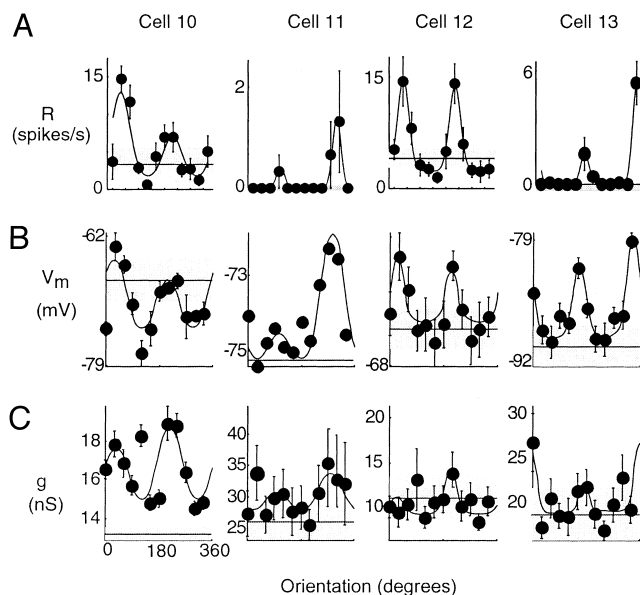


FIG. 12. Orientation tuning of the firing rate, of the membrane potential, and of the input conductance for 4 complex cells. *A*: spike responses. *B*: membrane potential responses. *C*: input conductance responses (only mean values are shown).

where the synaptic conductances are expressed relative to their value in the absence of visual stimulation. That is, in the absence of stimulation, we take the total conductance to be equal to the resting conductance, and the synaptic conductances to be zero.

Given Eq. 4, the visually driven membrane potential depends on the conductances as follows

$$V_{\text{visual}}(t) = [g_e(t)V_e + g_i(t)V_i + g_{rest}V_{rest}]/g(t) \quad (5)$$

where V_e and V_i are the equilibrium potentials for excitatory and inhibitory synaptic conductances.

We find the excitatory and inhibitory synaptic conductances, $g_e(t)$ and $g_i(t)$, by solving Eqs. 4 and 5. We set $V_e = 0$ mV and $V_i = -85$ mV. The latter is intermediate between the equilibrium potentials of GABA_A and GABA_B inhibitory channels. The remaining parameters in Eqs. 4 and 5 are known from the analysis described in the first part of the paper: V_{rest} is obtained from the membrane potential recordings without injected current, and g_{rest} , $g(t)$, and $V_{\text{visual}}(t)$ are obtained by fitting the plot of membrane potential versus injected current with a line as described in Eq. 3. Equations 4 and 5 are thus a system of two

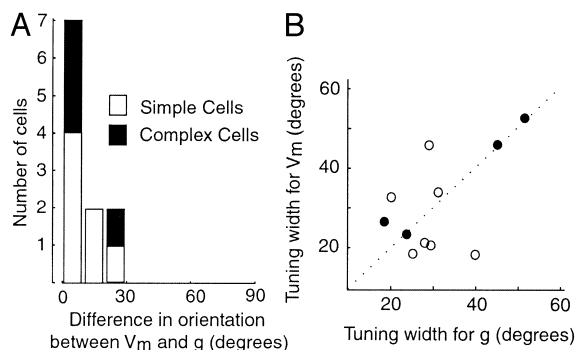


FIG. 13. Summary of the preferred orientations and tuning widths for the membrane potential and input conductance of the 11 cells measured with different orientations. *A*: difference in preferred orientation for the membrane potential and the input conductance. *B*: the half-width at half-height of tuning curves fitted to modulation (simple cells, \circ) and mean (complex cells, \bullet) of conductance (g) and membrane potential (V).

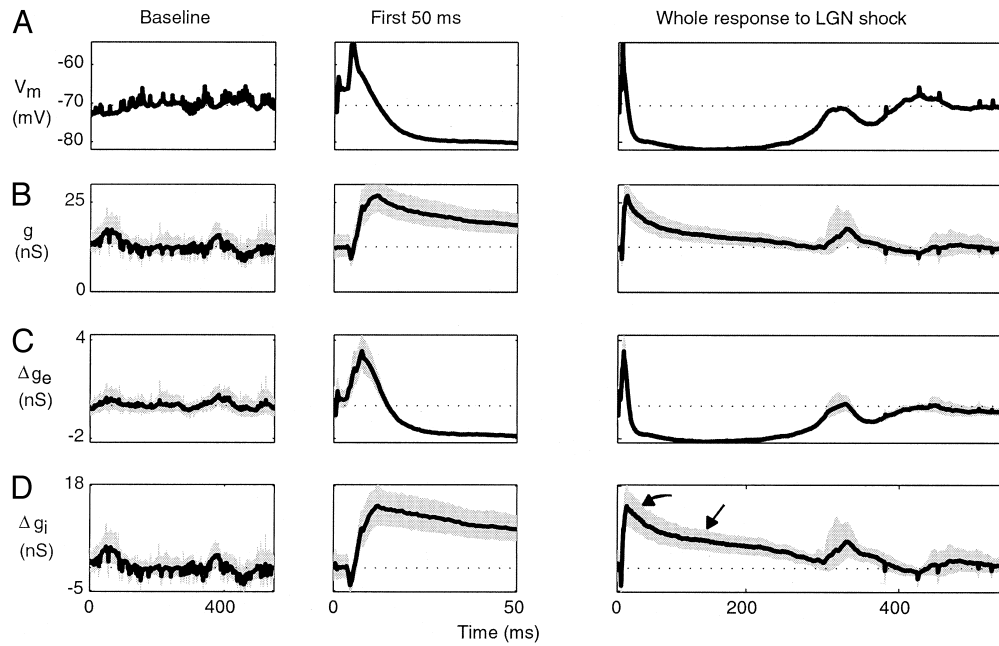


FIG. 14. Derivation of synaptic excitation and synaptic inhibition. Data taken from cortical responses to electrical shock of the lateral geniculate nucleus. *Left*: baseline (before shock) traces; *middle*: 1st 50 ms after shock; and *right*: 1st 500 ms after shock. \square , 95% confidence intervals; ---, resting values. *A*: membrane potential responses. *B*: input conductance. *C*: variation in excitatory synaptic conductance. *D*: variation in inhibitory synaptic conductance. *Cell 24*.

equations in two unknowns, $g_e(t)$ and $g_i(t)$, which can be solved at each point in time with simple linear methods.

As a validation of our methods, we first attempted to distinguish excitatory and inhibitory conductance changes evoked not by visual stimuli, but by electrical stimulation of the LGN because the conductance changes evoked by electrical stimuli are relatively well understood. An example of our results, obtained from a complex cell, is illustrated in Fig. 14. For this analysis, 10–100 responses to LGN shocks were averaged for each of 21 different injected currents. Figure 14, *left*, shows baseline recordings (without stimulation) and derived conductances. Figure 14, *middle* and *right*, shows the responses at two different time scales.

The excitatory and inhibitory conductance changes shown in *C* and *D* conform well to what one would expect from the response to electrical stimulation (e.g., Douglas et al. 1991a; Dreifuss et al. 1969; Pei et al. 1991). The excitatory conductance began rising 3–4 ms after the shock, reached its peak by 11 ms, decayed to its baseline value by 25 ms, and dropped below the baseline value for about 300 ms. Inhibitory conductance began to rise about 2–5 ms following the initial increase of the excitatory conductance, peaked at about 18–20 ms, and showed a very slow withdrawal, lasting about 300 ms, before returning to baseline values. The decay of the inhibitory conductance appeared to show two components, a fast component (left arrow) and a slow component (right arrow), which may

represent GABA_A and GABA_B components of the inhibitory response (Douglas et al. 1991a). Note that the long-lasting drop below baseline of the excitatory conductance occurs in parallel with the rise in inhibition. We attribute this to the concomitant decrease in activity in neighboring cortical cells, many of which presumably excite the recorded cell.

In the cell of Fig. 14, the total conductance rose by about 100% of its resting value, a change that is on the moderately high end of the spectrum of conductance increases we observed in responses to both visual and electrical stimulation in complex cells. The magnitude of conductance changes observed in response to electrical stimulation and the timing of their excitatory and inhibitory components are summarized in Table 2 for the eight complex cells and three simple cells studied.

Push-pull arrangement of excitation and inhibition

Having tested its validity with electrical stimuli, we then applied the decomposition method to the visually evoked excitatory and inhibitory conductances of a simple cell (Fig. 15). Figure 15, *left*, shows responses to blank stimuli, *right* shows responses to a drifting grating. This cell exhibits a property common to all the simple cells we analyzed: that is, excitatory and inhibitory conductances are modulated in counterphase, such that whenever one increases, the other decreases, and vice versa (Douglas et al. 1991b; Ferster 1988; Ferster and Ja-

TABLE 2. Conductance responses to electrical stimulation of the lateral geniculate nucleus

Type	<i>n</i>	Max Δg , %*	g_e timing, ms			g_i timing, ms		
			Onset	Peak	Decay	Onset	Peak	Decay
Simple	3	140 ± 80.8	1.8 ± 0.1	9.5 ± 0.9	23.0 ± 1.0	3.7 ± 0.3	13.7 ± 0.9	250 ± 10
Complex	8	46.3 ± 11.8	3.9 ± 0.2	11.5 ± 0.5	31.6 ± 2.9	7.2 ± 0.7	20.0 ± 1.4	280 ± 9

Values are means ± SE. * Max Δg is the maximal percent increase in input conductance over baseline conductance observed in the recordings.

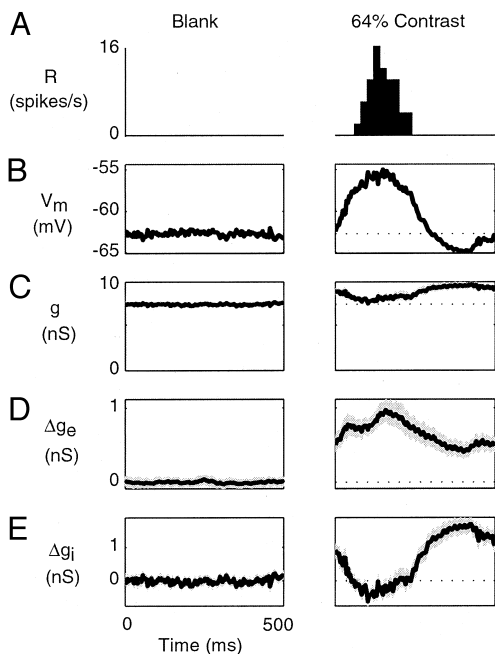


FIG. 15. Extraction of synaptic excitation and synaptic inhibition. We illustrate the process using 2 responses from a simple cell to blank stimuli (*left*) and drifting grating stimuli (*right*). The orientation of the stimulus shown on the right is 45° . Preferred orientation for cell is 75° . ---, resting values. *A*: spike rate responses. *B*: membrane potential responses. *C*: total input conductance. *D*: variation in excitatory synaptic conductance. *E*: variation in inhibitory synaptic conductance. *Cell 3*.

gadeesh 1992; Heggelund 1981; Palmer and Davis 1981). In *D* and *E*, the excitatory and inhibitory conductances induced by the stimulus show an approximately 180° difference in temporal phase. This difference has the effect of producing a very small modulation in total conductance (*C*) compared with the large modulation in membrane potential (*B*).

Examples of this push-pull arrangement of excitation and inhibition can be observed in the responses of two additional simple cells, displayed in Figs. 16 and 17. Similar to the cell in Fig. 15, these cells showed a push-pull organization in excitation and inhibition for orientations near the preferred. The excitatory and inhibitory conductances, however, were not always in exact counterphase. In the cell of Fig. 16, for example, excitatory and inhibitory components of conductance were in counterphase at an orientation of 270° , but at the preferred orientation (90°) they were only 60° out of phase. To compare the difference in phase between excitatory and inhibitory components of conductance, we measured this difference at each orientation for which modulation over time was significant. By averaging these measurements from all of our simple cells, we found the excitatory and inhibitory components were out of phase by an average of $153 \pm 14^\circ$ ($n = 7$).

It should be noted that the excitatory components of conductance do not descend below baseline levels, which supports the view that intracortical inhibition is the dominant or perhaps sole mechanism for generating troughs in membrane potential fluctuations, while withdrawal of baseline thalamic drive plays little or no role (Hirsch et al. 1998).

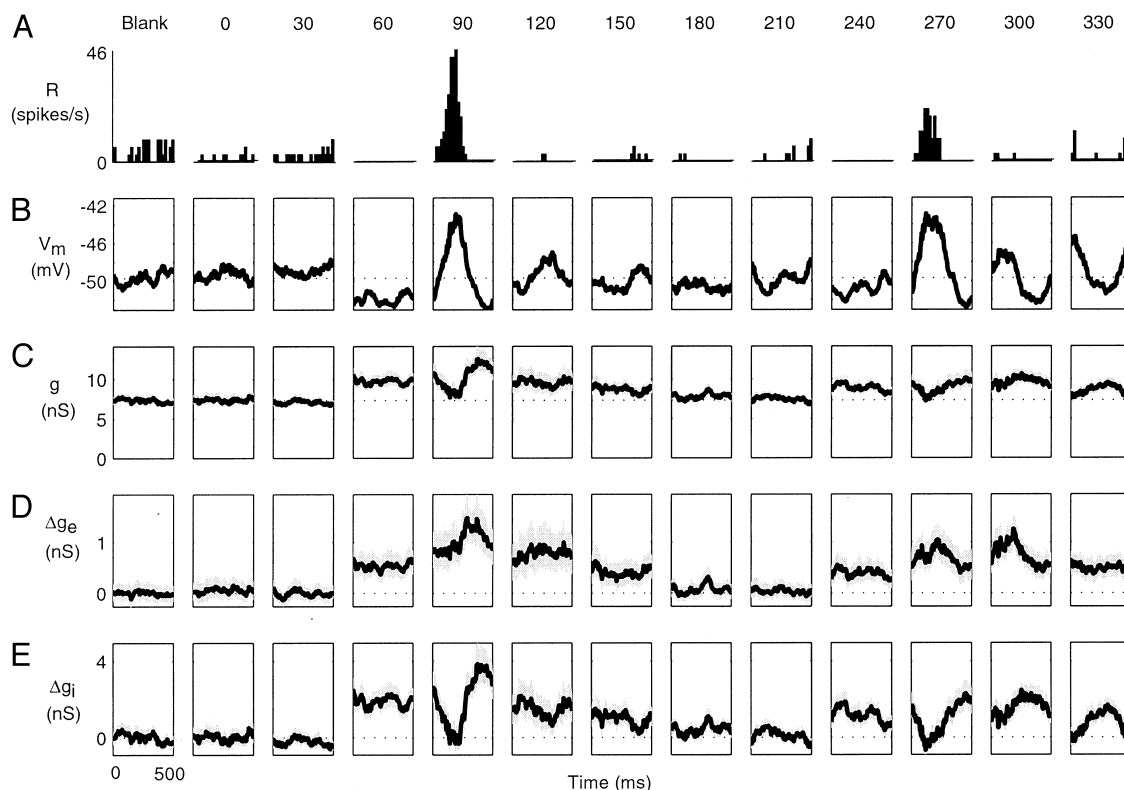


FIG. 16. Decomposition of input conductance into excitatory and inhibitory components for a simple cell. Responses are shown to a blank stimulus with 0% contrast followed by 64% contrast stimuli at 12 equally spaced orientations. *A*: spike responses. *B*: membrane potential responses. *C*: total input conductance. *D*: change in excitatory conductance from baseline. *E*: change in inhibitory conductance from baseline. *Cell 5*.

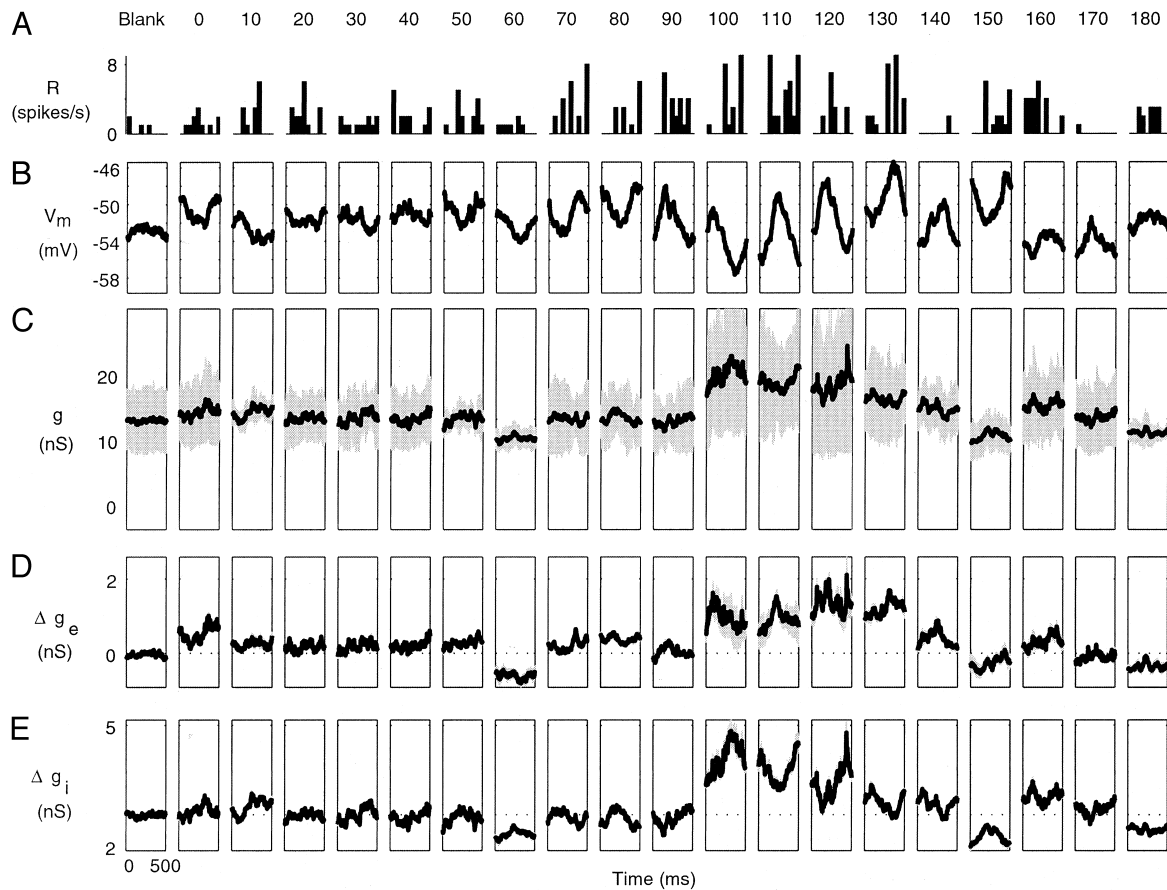


FIG. 17. Excitatory and inhibitory components of conductance for another simple cell. Measurements were taken at 10° intervals over 180° . Otherwise, the format is as in Fig. 16. *Cell 7*.

Orientation tuning of excitation and inhibition

Using measurements like those shown in Fig. 16, *D* and *E*, one can study the orientation tuning of synaptic excitation and inhibition. In the cell in that figure, both excitatory and inhibitory conductances increased at or near the preferred orientation and were modulated over time as was total conductance. The magnitude of the increase in inhibitory conductance, however, was greater than for excitatory conductance. Therefore the modulation in total conductance was most similar to the modulation in inhibitory conductance, with the peak conductance coinciding with the trough in membrane potential.

Similar measurements for the seven simple cells in our sample are shown in Fig. 18, which shows tuning curves for synaptic excitation and inhibition. The cell in Fig. 16 is illustrated in the bottom right column. Excitatory conductances (*A* and *C*) were generally lower in magnitude than inhibitory conductances (*B* and *D*). With the exception of *cell 2*, where the inhibition was mostly tonic, both excitation and inhibition tended to be modulated in time. In the majority of cases, visual stimulation increased the synaptic conductances above baseline. Modulations in synaptic conductances thus were accompanied by increases in mean conductance. As a result, with the exception of *cell 6*, the mean component for both excitation and inhibition (\odot) was tuned just like the modulation component (\bullet). Excitation and inhibition were both tuned for orientation but could in some cells be affected by stimuli of all orientations. Only in *cells 2* and *5* did stimuli orthogonal to the

preferred elicit no increases in excitatory or inhibitory conductance. In the other cells, the tuning curves for the conductances were generally elevated with respect to the values at rest.

The orientation tuning of the excitatory and inhibitory synaptic inputs appears to be very similar. In turn, this orientation tuning is rather similar to that of the membrane potential and of the total conductance (Fig. 10). To compare the preferred orientation and tuning width of excitation and inhibition, we fitted the descriptive tuning curve (*Eq. 2*) to the mean and modulation of the excitatory and inhibitory conductances. We then compared the parameters of the function with those obtained from fitting the firing rate, the membrane potential, and the input conductance. Comparisons between tuning widths for excitatory conductance, inhibitory conductance, and membrane potential are shown in Fig. 19 for the seven simple cells studied. The tuning widths of excitatory and inhibitory synaptic conductances were not systematically different (*A*), with a mean difference of only $0.5 \pm 1.8^\circ$ ($n = 7$). In addition, the tuning widths of the synaptic conductances were in the same range as those of the membrane potential (*B*): the tuning width of the excitatory synaptic conductance differed from that of the membrane potential by only $3.3 \pm 6.4^\circ$ ($n = 7$) in simple cells. The tuning width of the inhibitory synaptic conductance differed from that of membrane potential (*C*) by only $3.2 \pm 3.5^\circ$.

The close agreement in tuning widths of excitatory and inhibitory conductances that we have measured in Fig. 19 extends previous observations that excitatory and inhibitory

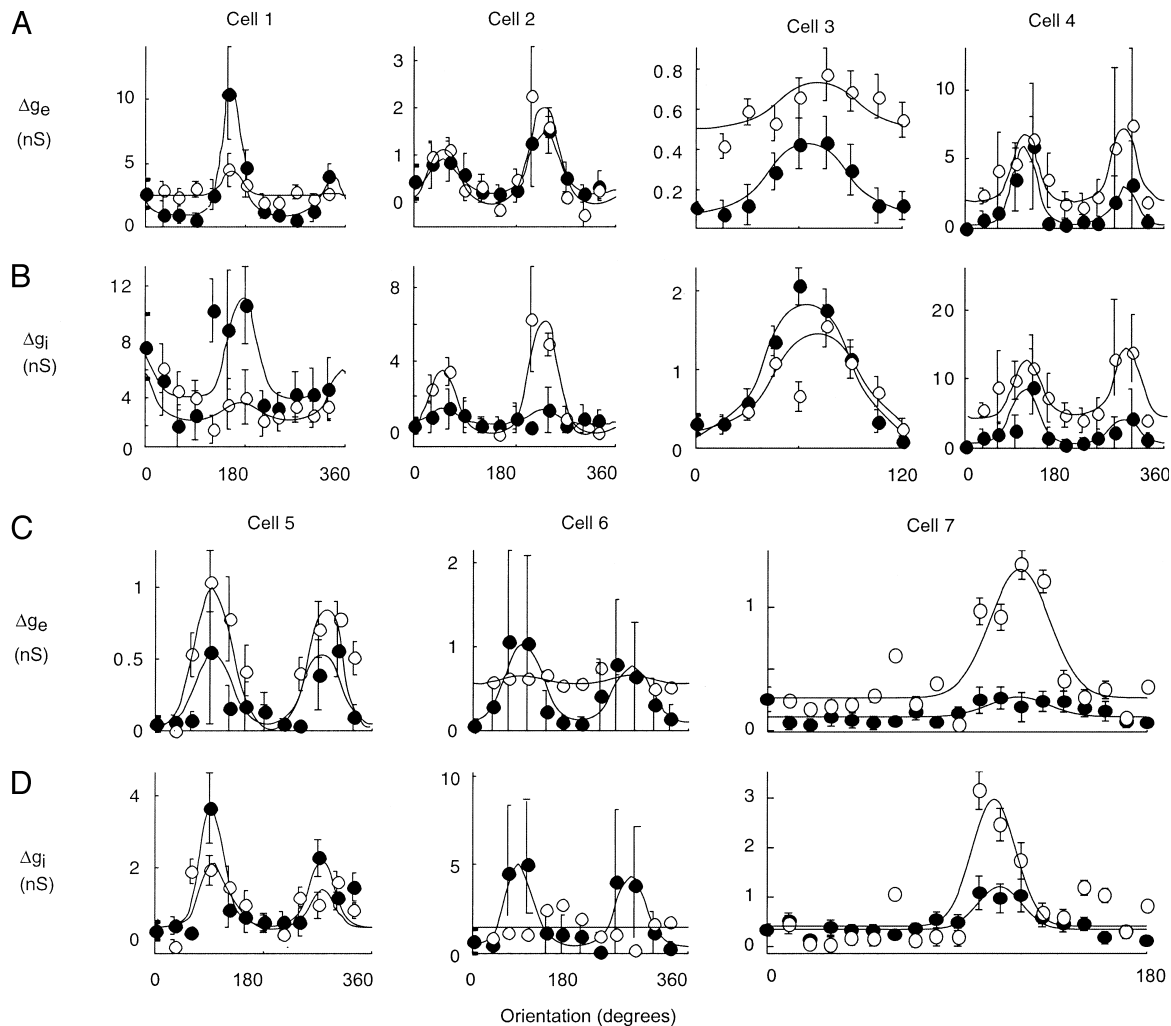


FIG. 18. Orientation tuning of excitation and inhibition for 7 simple cells. Error bars represent 1 SE. *A* and *C*: tuning of synaptic excitation. *B* and *D*: tuning of synaptic inhibition. Symbols indicate mean (\circ) and modulation (\bullet) of excitatory and inhibitory synaptic conductances at each orientation. Orientation tuning for potential and total conductance for these cells is shown in Fig. 10.

postsynaptic potentials (EPSPs and IPSPs) have similar orientation preference (Ferster 1986). Although the spacing between orientations in our stimuli was rather coarse (30° for 5 cells, 15° for 1 cell, 10° for 1 cell), tuning widths for all relevant parameters were sufficiently large (i.e., half-width greater than 17°) to adequately constrain a Gaussian fit at our sampling resolution. Our measurements therefore should have been able to detect a systematic difference in tuning width or preferred orientation between excitation and inhibition. The close agreement between excitation and inhibition suggests that intracortical excitation and inhibition originate from cells that are similarly tuned and could explain previous results (Chung and

Ferster 1998; Ferster et al. 1996; Nelson et al. 1994) that the orientation tuning of cat V1 simple cells is not significantly sharpened by synaptic inhibition.

DISCUSSION

In agreement with Borg-Graham et al. (1998) and Hirsch et al. (1998), we have found that the input conductance of cells in primary visual cortex increases significantly (20–300%) during the presentation of drifting gratings at the preferred orientation. In addition, we have found that these increases in input conductance are well tuned for stimulus orientation and that

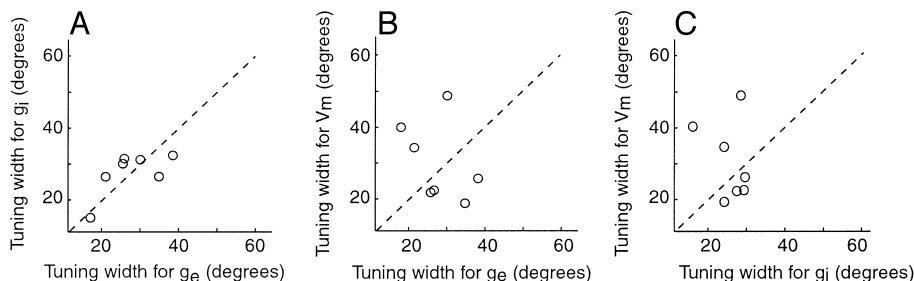


FIG. 19. Summary of the tuning widths for the excitatory and inhibitory conductance of the 7 simple cells tested with different orientations. Panels show the half-width at half-height of tuning curves fitted to modulation. *A*: tuning width of excitatory conductance vs. tuning width of inhibitory conductance. *B*: tuning width of excitatory conductance vs. tuning width of membrane potential. *C*: tuning width of inhibitory conductance vs. tuning width of membrane potential.

their preferred orientation and tuning widths are nearly identical to those of the membrane potential responses.

These results argue against both of the models depicted in Fig. 1. The results argue against the veto model (*A*) because it predicts that a cell's conductance should be highest for the orientations that are most different from the preferred orientation (Koch and Poggio 1985). The results argue against the normalization model (*B*) because it predicts that conductance should be independent of stimulus orientation (Carandini and Heeger 1994; Carandini et al. 1997, 1999). The increases in input conductance that we measured do constitute a gain-control mechanism that decreases the responsiveness of the cells at high stimulus contrast, but this mechanism is orientation selective and thus does not depend purely on visual contrast.

Measuring input conductance in vivo

While our data agree with recent measurements of visually evoked changes in conductance (Borg-Graham et al. 1998; Hirsch et al. 1998), earlier measurements of input conductance during visual stimulation, even with stimuli of optimal orientation, resulted in lower values. Guided by the large conductance changes observed by Borg-Graham et al. (1998) and Hirsch et al. (1998), we have examined the factors that may have resulted in lower estimates in previous studies. These estimates ranged from a lack of measurable increase (Carandini and Ferster 1997; Douglas et al. 1988; Pei et al. 1991), to 16% (Berman et al. 1991) or 25% (Ferster and Jagadeesh 1992). Most likely, the reasons for the divergence in estimates lie in the differences in methods for visual stimulation and more importantly in differences in estimating the series resistance of the electrodes.

Indeed, the most critical steps in measuring the input resistance from single-electrode, whole cell recordings in vivo is the correct estimation of the electrode's access, or series, resistance. The change in potential evoked by an injected current pulse, which is used to measure input resistance, is equal not to the injected current multiplied by the cell's input resistance but to the current times the sum of the input and electrode resistances. With in vitro recordings, the components of the response to a current pulse belonging to the electrode and to the cell are easy to distinguish. The electrode and cell time constants are so different that the electrode capacitance has finished charging by the time the membrane capacitance has just begun to do so. It is therefore a simple matter to "balance the bridge" by eye, subtracting out the electrode component and thereby reaching an accurate estimate of the cell's input resistance.

The situation in vivo is different. The time constant of the electrode is larger in vivo than in vitro. First, the capacitance of the electrode is higher because its shank is embedded in several millimeters of tissue and agar. Second, the resistance of the electrode is increased as its tip passes through many hundreds of micrometers of tissue. The time constant of the electrode therefore approaches that of the cell, making it difficult to distinguish the electrode and cell components of the response to a current pulse, thereby requiring more quantitative methods for "balancing the bridge." This requirement is most likely the source of the error in our own previous study of conductance (Carandini and Ferster 1997) where we used only the on-line bridge-balance technique for compensating for electrode series

resistance and arrived at the conclusion that visual stimulation has little effect on conductance. Without using the more quantitative methods used here, we likely did not properly correct for the electrode resistance.

In this paper, we have adopted two independent methods that together allow precise measurements of the electrode resistance. The methods also provide correction for drifts in electrode resistance over time. They achieve a precision of better than 10%, over which range none of the conclusions of the study are significantly affected. This uncertainty in electrode resistance, and the corresponding uncertainty in membrane resistance, may yield an additional increase in the size of confidence intervals for measurements of input conductance.

One assumption that enters into our measurement of conductance is that the current-voltage relationship in the recorded neurons is linear. The *I-V* curves that we measured tend to bear this assumption out, which is somewhat surprising given the large number of voltage-sensitive conductances present in neurons. We have used hyperpolarizing currents for most of our tests to minimize the involvement of active currents. Nevertheless even when the cells were spiking, the *I-V* relationship was approximately linear, suggesting that the active currents underlying the spike are concentrated in the initial segment or even the first node of Ranvier (Colbert and Johnston 1996), away from the soma. That simple cells, at least, behave relatively linearly is borne out by their responses to visual stimulation, which are in some aspects quite linear (Carandini and Ferster 2000; Jagadeesh et al. 1993, 1997).

Distinguishing excitation and inhibition

In addition to measuring total input conductance, we have employed a simple method for deriving the excitatory and inhibitory components of conductance changes underlying visual responses based on the assumption that such changes are synaptic in origin. In this respect, one simplification in our model is our use of a single type of synaptic inhibition. Cortical cells have both GABA_A and GABA_B receptors, which are permeable to K⁺ and Cl⁻ ions. Normally these channels would have equilibrium potentials near -65 and -100 mV. But the solution in our electrodes, which contains little chloride, would hyperpolarize the GABA_A equilibrium potential. We have therefore chosen the equilibrium potential for our inhibitory conductance (V_i) to be -85 mV, somewhere between GABA_A and GABA_B. The equilibrium potential for the excitatory conductance (V_e) was set to 0 mV, close to the equilibrium potential of glutamatergic synapses. We have repeated all of the analyses of excitatory and inhibitory components of conductance, varying the values of V_e and V_i by 10 mV in either direction. These changes did not significantly affect any of the basic conclusions of the study, either for electrically or visually evoked responses, and yielded distributions of excitation and inhibition that were within 5% of each other.

One potential limitation of our technique for deriving excitatory and inhibitory conductances arises from the possibility that some synaptic inputs are located in electrotonically distant portions of the dendrites. In that case, our current-clamp measurements would suffer the same problem that voltage-clamp recordings do when the space clamp is inadequate: the current-induced changes in potential would be different in different parts of the dendritic tree and soma. These differences would in

turn mean that the excitatory synaptic currents in the dendrites would reverse only when the potential in the soma was higher than 0 mV. Similarly, inhibitory synaptic currents in the dendrites would reverse only when the potential in the soma was lower than -65 or -100 mV. We would then mistake a portion of the excitatory conductance for a negative inhibitory conductance, and vice versa. There are hints of this type of error in the responses to electrical stimulation (Fig. 14). But the time course and relative magnitude of the calculated conductances in this case are similar to what would be expected. Furthermore this type of error could not generate negative inhibitory conductances that are larger in amplitude than the excitatory conductances. Since the derived inhibitory conductances are two to three times larger than the excitatory conductances, we conclude that errors arising from inadequate space clamp are not large enough to affect our results significantly.

The technique used here to derive excitatory and inhibitory conductances offers significant advantages over other methods. For example, in the study of Pei et al. (1994), tuning curves for excitation and inhibition were inferred from the hyperpolarization and depolarization amplitudes. Such techniques, which rely solely on membrane potential traces, would miss concurrent excitation and inhibition. This would lead to a significant underestimation of inhibitory responses at orientations where excitation is strongest. Similar considerations apply to the work of Volgushev et al. (1992, 1993), who analyzed membrane potential responses to visual stimuli, in one case during injection of current. Finally, there may have been flaws in the approach of Ferster and Jagadeesh (1992), who attempted to measure conductance changes by observing changes in the amplitude of a test EPSP evoked by electrical stimulation of the LGN. Because the test EPSPs were so brief, the measurements were likely dominated by membrane capacitance rather than resistance.

Push-pull arrangement of excitation and inhibition

While both excitation and inhibition are evoked by the preferred stimulus, in the subfields of simple cells they are spatially segregated. As Hubel and Wiesel (1962) suggested, on regions receive off inhibition, and off regions receive on inhibition in a push-pull arrangement. The first description of push-pull organization in intracellular recordings focused on hyperpolarizing IPSPs evoked by flashing bars (Ferster 1988). More recently, large changes in conductance associated with these IPSPs have been described by Borg-Graham et al. (1998) and by Hirsch et al. (1998). In agreement with Hirsch, we find that the hyperpolarizing off responses in the on region (and conversely, on responses in the off region) are dominated by the increase in inhibitory inputs with little contribution from the withdrawal of excitation. The use of sinusoidal gratings has allowed us to make careful measurements of the relative placement of the excitatory and inhibitory inputs within the subfields, where we find a surprisingly accurate push-pull arrangement. The 153° average displacement in the spatial phases of the inhibition and excitation represents less than $1/6$ of a stimulus cycle difference from a perfect counterphase arrangement. Given that the stimulus is at the optimal spatial frequency, such that the spacing of the stimulus bars is comparable to the spacing of the subfields, this 153° offset means that

the on inhibitory inputs are superimposed with OFF excitatory inputs (and vice versa) with an error of less than 20% of the receptive field width. This 20% displacement, given the relatively small sample size, cannot be reliably distinguished from perfect counterphase. This small difference might also be accounted for by a difference in temporal phase of excitatory and inhibitory inputs.

Our results agree closely with a model of cat simple cell function in which a spatial push-pull arrangement of on and off excitation and inhibition is a prominent feature. Troyer et al. (1998) have applied push-pull inhibition to the feedforward models of orientation selectivity (Hubel and Wiesel 1962) to correct the feedforward model's failure to predict the contrast invariance of orientation selectivity. Their model makes a number of predictions that are borne out by our results. First, it predicts an identical orientation tuning of excitatory and inhibitory conductance (e.g., Troyer 1998, Fig. 10). Second, it predicts an identical orientation tuning of the modulation of membrane potential and modulation of conductance. Third, it predicts conductance changes at the preferred orientation (about 100%) similar to those that we report.

Tuning of inhibition

We found that excitation and inhibition have similar tuning for orientation, so that inhibition is unlikely to sharpen the tuning conveyed by the excitatory inputs. These results are at odds with a number of studies suggesting that intracortical inhibition is more broadly tuned than excitation and thus helps in establishing the orientation tuning of the cells (Ben-Yishai et al. 1995; Blakemore and Tobin 1972; Creutzfeldt et al. 1974; Hata et al. 1988; Sillito 1979; Somers et al. 1995; Sompolinsky and Shapley 1997).

More recently, Ringach et al. (1998) have suggested that inhibition would be most effective in sharpening orientation tuning when its tuning width is only slightly greater than that of excitation. Inspection of Fig. 19 does not support such an arrangement. There does not appear to be any systematic difference between the tuning width of excitation and inhibition. On the other hand, this figure plots the tuning widths of combined fits to mean and modulation. It might be that individual tuning curves for the mean or modulation components of excitation might be wider than their counterparts for excitation. Figure 18, however, again shows no obvious systematic indication of such an effect.

In most cells we did observe increases in membrane conductance for stimuli of all orientations. These increases in conductance may go some way toward explaining the suppression effects measured with plaids obtained with two gratings differing in orientation (Bonds 1989; Carandini et al. 1999; Gizzi et al. 1990; Morrone et al. 1982). In addition, our data cannot rule out the possibility that broadly tuned inhibition may be operative in cat complex cells or in cells of other species such as the primate (Ringach et al. 1997).

While our results are not consistent with a broadly tuned inhibition, they do suggest an important role for intracortical excitation in establishing orientation selectivity, as proposed by a number of models, both recurrent (Ben-Yishai et al. 1995; Chance et al. 1999; Douglas et al. 1991a, 1995; Martin 1988; Ringach et al. 1997; Somers et al. 1995) and feedforward (Troyer et al. 1998). According to these models, cortical cells

receive substantial excitatory input from other cortical cells that are similarly tuned. Our result that the mean input conductance of simple cells is increased more by stimuli of the optimal orientation than by stimuli of other orientations is consistent with this view. To see why this is the case, it may help to consider the predictions of a basic linear feedforward model of orientation tuning in simple cells (Ferster 1987; Hubel and Wiesel 1962). Imagine that changes in input conductance of a cell resulted from a weighted sum of the responses of properly aligned unoriented cells in the LGN. In principle, the weights could be positive and negative, reflecting both synaptic excitation and inhibition, possibly through interneurons. Because the LGN cells are not oriented, the orientation of the stimulus affects the relative timing—but not the size—of their responses. When the stimulus has the preferred orientation, these responses would be synchronized so that their weighted sum is strongly modulated. But the *mean* input conductance generated by the geniculate input would not be tuned for stimulus orientation because the mean response of the individual cells would be the same for all orientations.

If we are correct in our assumption that the changes in input conductance are entirely synaptic, then our finding that the mean conductance of simple cells is often tuned for stimulus orientation indicates that either simple cells integrate their inputs nonlinearly or they receive input from cells that have similar orientation tuning. These, of course, would have to be other cortical cells. The first explanation is supported by mounting evidence for nonlinearities operating at the synaptic (e.g., Abbott et al. 1997; Markram and Tsodyks 1996) or dendritic level (Mel et al. 1998). The second explanation is supported by evidence that the cortical circuitry contributes a two- to threefold amplification of the responses of simple cells (Chung and Ferster 1998; Ferster et al. 1996; Martin 1988). These explanations are not mutually exclusive, and further experiments will be needed to determine their validity.

We thank L. Borg-Graham and J. Hirsch for helpful suggestions on bridge-balancing techniques and K. Martin and T. Troyer for comments on the manuscript.

This work was supported by National Eye Institute Grant EY-04726 to D. Ferster. J. S. Anderson was supported by NEI Training Grant EY-07128. M. Carandini was partly supported by a Howard Hughes Medical Institute investigatorship to J. A. Movshon.

REFERENCES

- ABBOTT LF, VARELA JA, SEN K, AND NELSON SB. Synaptic depression and cortical gain control. *Science* 275: 220–224, 1997.
- BEN-YISHAI R, OR RLB, AND SOMPOLINSKY H. Theory of orientation tuning in the visual cortex. *Proc Natl Acad Sci USA* 92: 3844–3848, 1995.
- BERMAN NJ, DOUGLAS RJ, MARTIN KAC, AND WHITTERIDGE D. Mechanisms of inhibition in cat visual cortex. *J Physiol (Lond)* 440: 697–722, 1991.
- BLAKEMORE C AND TOBIN EA. Lateral inhibition between orientation detectors in the cat's visual cortex. *Exp Brain Res* 15: 439–440, 1972.
- BLANTON MG, LO TURCO JJ, AND KRIEGSTEIN AR. Whole cell recording from neurons in slices of reptilian and mammalian cerebral cortex. *J Neurosci Methods* 30: 203–210, 1989.
- BONDS AB. Role of inhibition in the specification of orientation selectivity of cells in the cat striate cortex. *Vis Neurosci* 2: 41–55, 1989.
- BORG-GRAHAM LJ, MONIER C, AND FRÉGNAC Y. Visual input evokes transient and strong shunting inhibition in visual cortical neurons. *Nature* 393: 369–373, 1998.
- CARANDINI M, ANDERSON J, AND FERSTER D. Excitatory and inhibitory conductance changes in simple cells of cat visual cortex (Abstract). *Eur J Neurosci* 10, Suppl 10: 331, 1998a.
- CARANDINI M, ANDERSON J, AND FERSTER D. Membrane conductance changes in simple cells of cat visual cortex. *Perception (Suppl)* 7: 41, 1998b.
- CARANDINI M, ANDERSON J, AND FERSTER D. Tuning of membrane conductance changes in simple cells of the cat striate cortex. *Soc Neurosci Abstr* 24: 766, 1998c.
- CARANDINI M AND FERSTER D. A tonic hyperpolarization underlying contrast adaptation in cat visual cortex. *Science* 276: 949–952, 1997.
- CARANDINI M AND FERSTER D. Orientation tuning of membrane potential and firing rate in cat primary visual cortex. *J Neurosci* 20: 470–484, 2000.
- CARANDINI M AND HEEGER DJ. Summation and division by neurons in primate visual cortex. *Science* 264: 1333–1336, 1994.
- CARANDINI M, HEEGER DJ, AND MOVSHON JA. Linearity and normalization in simple cells of the macaque primary visual cortex. *J Neurosci* 17: 8621–8644, 1997.
- CARANDINI M, HEEGER DJ, AND MOVSHON JA. Linearity and gain control in V1 simple cells. In: *Cerebral Cortex. Models of Cortical Circuits*, edited by Uliniski PS, Jones EG, and Peters A. New York: Kluwer Academic/Plenum, 1999, vol. 13, p. 401–443.
- CELEBRINI S AND NEWSOME WT. Microstimulation of extrastriate area MST influences performance on a direction discrimination task. *J Neurophysiol* 73: 437–448, 1995.
- CHANCE FS, NELSON SB, AND ABBOTT LF. Complex cells as cortically amplified simple cells. *Nat Neurosci* 2: 277–282, 1999.
- CHUNG S AND FERSTER D. Strength and orientation tuning of the thalamic input to simple cells revealed by electrically evoked cortical suppression. *Neuron* 20: 1177–1189, 1998.
- COLBERT CM AND JOHNSTON, D. Axonal action-potential initiation and Na⁺ channel densities in the soma and axon initial segment of subicular pyramidal neurons. *J Neurosci* 16: 6676–6686, 1996.
- CREUTZFELDT OD, KUHN U, AND BENEVENTO LA. An intracellular analysis of visual cortical neurones to moving stimuli: responses in a co-operative neuronal network. *Exp Brain Res* 21: 251–274, 1974.
- DOUGLAS RJ, KOCH C, MAHOWALD M, MARTIN KAC, AND SUAREZ HH. Recurrent excitation in neocortical circuits. *Science* 269: 981–985, 1995.
- DOUGLAS RJ, MARTIN KAC, AND WHITTERIDGE D. Selective responses of visual cortical cells do not depend on shunting inhibition. *Nature* 332: 642–644, 1988.
- DOUGLAS RJ, MARTIN KAC, AND WHITTERIDGE D. A functional microcircuit for cat visual cortex. *J Physiol (Lond)* 440: 735–769, 1991a.
- DOUGLAS RJ, MARTIN KAC, AND WHITTERIDGE D. An intracellular analysis of the visual responses of neurones in cat visual cortex. *J Physiol (Lond)* 440: 659–696, 1991b.
- DREIFUSS JJ, KELLY JS, AND KRNEVIC K. Cortical inhibition and gamma-aminobutyric acid. *Exp Brain Res* 9: 137–154, 1969.
- EFRON B AND TIBSHIRANI RJ. *An Introduction to the Bootstrap*. New York: Chapman and Hall, 1993, vol. 57.
- FERSTER D. Orientation selectivity of synaptic potentials in neurons of cat primary visual cortex. *J Neurosci* 6: 1284–1301, 1986.
- FERSTER D. The origin of orientation selective EPSPs in simple cells of cat visual cortex. *J Neurosci* 7: 1780–1791, 1987.
- FERSTER D. Spatially opponent excitation and inhibition in simple cells of the cat visual cortex. *J Neurosci* 8: 1172–1180, 1988.
- FERSTER D, CHUNG S, AND WHEAT HS. Orientation selectivity of thalamic input to simple cells of cat visual cortex. *Nature* 380: 249–252, 1996.
- FERSTER D AND JAGADEESH B. EPSP-IPSP interactions in cat visual cortex studied with in vivo whole-cell patch recording. *J Neurosci* 12: 1262–1274, 1992.
- GIZZI MS, KATZ E, SCHUMER RA, AND MOVSHON JA. Selectivity for orientation and direction of motion of single neurons in cat striate and extrastriate visual cortex. *J Neurophysiol* 63: 1529–1543, 1990.
- HATA Y, TSUMOTO T, SATO H, HAGIHARA K, AND TAMURA H. Inhibition contributes to orientation selectivity in visual cortex of cat. *Nature* 335: 815–817, 1988.
- HEEGER DJ. Normalization of cell responses in cat striate cortex. *Vis Neurosci* 9: 181–197, 1992.
- HEGGLUND P. Receptive-field organization of simple cells in cat striate cortex. *Exp Brain Res* 42: 89–98, 1981.
- HIRSCH JA, ALONSO JM, REID RC, AND MARTINEZ LM. Synaptic integration in striate cortical simple cells. *J Neurosci* 18: 9517–9528, 1998.
- HUBEL DH AND WIESEL TN. Receptive fields, binocular interaction and functional architecture in the cat's visual cortex. *J Physiol (Lond)* 160: 106–154, 1962.
- JAGADEESH B, WHEAT HS, AND FERSTER D. Linearity of summation of synaptic potentials underlying direction selectivity in simple cells of the cat visual cortex. *Science* 262: 1901–1904, 1993.

- JAGADEESH B, WHEAT HS, KONTSEVICH LL, TYLER CW, AND FERSTER D. Direction selectivity of synaptic potentials in simple cells of the cat visual cortex. *J Neurophysiol* 78: 2772–2789, 1997.
- KOCH C. *Biophysics of Computation*. New York: Oxford, 1999.
- KOCH C AND POGGIO T. The synaptic veto mechanism: does it underlie direction and orientation selectivity in the visual cortex? In: *Models of the Visual Cortex*, edited by Dobson VG and Rose D. New York: Wiley, 1985, p. 408–419.
- MARKRAM H AND TSODYKS M. Redistribution of synaptic efficacy between neocortical pyramidal neurons. *Nature* 382: 807–810, 1996.
- MARTIN KAC. From single cells to simple circuits in the cerebral cortex. *Q J Exp Physiol* 73: 637–702, 1988.
- MEL BW, RUDERMAN DL, AND ARCHIE KA. I. Translation-invariant orientation tuning in visual “complex” cells could derive from intradendritic computations. *J Neurosci* 18: 4325–4334, 1998.
- MORRONE MC, BURR DC, AND MAFFEI L. Functional implications of cross-orientation inhibition of cortical visual cells. I. Neurophysiological evidence. *Proc R Soc Lond B Biol Sci* 216: 335–354, 1982.
- MOVSHON JA, THOMPSON ID, AND TOLHURST DJ. Spatial summation in the receptive fields of simple cells in the cat’s striate cortex. *J Physiol (Lond)* 283: 53–77, 1978.
- NEHER E. Correction for liquid potentials in patch clamp experiments. In: *Methods in Enzymology: Ion Channels*, edited by Rudy B and Iverson LE. New York: Academic, 1992.
- NELSON S, TOTH L, SHETH B, AND SUR M. Orientation selectivity of cortical neurons during intracellular blockade of inhibition. *Science* 265: 774–777, 1994.
- PALMER LA AND DAVIS TL. Receptive-field structure in cat striate cortex. *J Neurophysiol* 46: 260–276, 1981.
- PEI X, VIDYASAGAR TR, VOLGUSHEV M, AND CREUTZFELDT OD. Receptive field analysis and orientation selectivity of postsynaptic potentials of simple cells in cat visual cortex. *J Neurosci* 14: 7130–7140, 1994.
- PEI X, VOLGUSHEV M, VIDYASAGAR TR, AND CREUTZFELDT OD. Whole cell recording and conductance measurements in cat visual cortex in-vivo. *Neuroreport* 2: 485–488, 1991.
- RINGACH DL. Tuning of orientation detectors in human vision. *Vision Res* 38: 963–972, 1998.
- RINGACH DL, HAWKEN MJ, AND SHAPLEY R. Dynamics of orientation tuning in macaque primary visual cortex. *Nature* 387: 281–284, 1997.
- SILLITO AM. Inhibitory mechanisms influencing complex cell orientation selectivity and their modification at high resting discharge levels. *J Physiol (Lond)* 289: 33–53, 1979.
- SKOTTUN BC, DE VALOIS RL, GROSOF DH, MOVSHON JA, ALBRECHT DG, AND BONDS AB. Classifying simple and complex cells on the basis of response modulation. *Vision Res* 31: 1079–1086, 1991.
- SOMERS DC, NELSON SB, AND SUR M. An emergent model of orientation selectivity in cat visual cortical simple cells. *J Neurosci* 15: 5448–5465, 1995.
- SOMPOLINSKY H AND SHAPLEY R. New perspectives on the mechanisms for orientation selectivity. *Curr Opin Neurobiol* 7: 514–522, 1997.
- SPRUSTON N, SCHILLER Y, STUART G, AND SAKMANN B. Activity-dependent action potential invasion and calcium influx into hippocampal CA1 dendrites. *Science* 268: 297–300, 1995.
- TROYER TW, KRUKOWSKI AE, PRIEBE NJ, AND MILLER KD. Contrast-invariant orientation tuning in cat visual cortex: thalamocortical input tuning and correlation-based intracortical connectivity. *J Neurosci* 18: 5908–5927, 1998.
- VOLGUSHEV M, PEI X, VIDYASAGAR TR, AND CREUTZFELDT OD. Postsynaptic potentials in cat visual cortex: dependence on polarization. *Neuroreport* 3: 679–682, 1992.
- VOLGUSHEV M, PEI X, VIDYASAGAR TR, AND CREUTZFELDT OD. Excitation and inhibition in orientation selectivity of cat visual cortex neurons revealed by whole-cell recordings in vivo. *Vis Neurosci* 10: 1151–1155, 1993.